2006

Introduction of control pins in the vicinity of missile fins for roll and yaw control

Jing Pei

INTRODUCTION OF CONTROL PINS IN THE VICINITY OF MISSILE FINS FOR ROLL AND YAW CONTROL

by

JING PEI

A THESIS

Submitted in partial fulfillment of the requirements
for the degree of Master of Science in Engineering
in
The Department of Mechanical and Aerospace Engineering
to
The School of Graduate Studies
of
The University of Alabama in Huntsville

HUNTSVILLE, ALABAMA

2006

In presenting this thesis in partial fulfillment of the requirements for a master's degree from The University of Alabama in Huntsville, I agree that the Library of this University shall make it freely available for inspection. I further agree that permission for extensive copying for scholarly purposes may be granted by my advisor or, in his/her absence, by the Chair of the Department or the Dean of the School of Graduate Studies. It is also understood that due recognition shall be given to me and to The University of Alabama in Huntsville in any scholarly use which may be made of any material in this thesis.

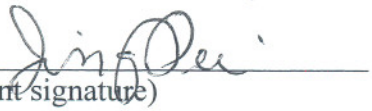

(student signature) 10/1/06 (date)

THESIS APPROVAL FORM

Submitted by Jing Pei in partial fulfillment of the requirements for the degree of Master of Science in Mechanical and Aerospace Engineering and accepted on behalf of the Faculty of the School of Graduate Studies by the thesis committee.

We, the undersigned members of the Graduate Faculty of The University of Alabama in Huntsville, certify that we have advised and/or supervised the candidate on the work described in this thesis. We further certify that we have reviewed the thesis manuscript and approve it in partial fulfillment of the requirements of the degree of Master of Science in Mechanical and Aerospace Engineering.

9/22/06
Committee Chair
(Date)

9/25/06

9/25/06

Department Chair

College Dean

10/19/06
Graduate Dean

ABSTRACT

The School of Graduate Studies
The University of Alabama in Huntsville

Degree Master of Science College /Dept. Mechanical and Aerospace Engineering

Name of Candidate Jing Pei

Title Introduction of Control Pins in the Vicinity of Missile Fins for Roll and Yaw Control Purposes

A recent study performed by the United States Army Research Laboratory has shown placement of diametrically opposed pins in the vicinity of missile fins is capable of producing a roll torque. To perform a follow up investigation on the project, an opposing pin model was created to determine whether a yaw moment instead of roll torque could be imposed on the projectile. A Matlab code was written to estimate the roll torque and fin normal force generated by the two pin configurations. The code was calibrated and verified by results from Computational Fluid Dynamics and spark range test data. The effect of the pin length, radius, and placement on the roll torque and normal force were investigated. Finally, trajectory simulations were performed in PRODAS to predict the roll and yaw performances of the projectile as it reaches a downrange distance of 100 m.

Abstract Approval: Committee Chair _____ 9/22/05 (Date)

Department Chair _____

Graduate Dean _____ 10/19/06

ACKNOWLEDGMENTS

I wish to thank my advisor, Dr. Landrum, for giving me the opportunity to work on this project. I would like to thank Olivier Demaneuf, Han Madhanabharatam, and the ESI support group for their assistance in my CFD simulations. I would also like to thank Jason Cassibry for his help with Matlab programming. I also would like to thank Brian Atkin for trying to set up a flight test for my experiment. Finally, I would like to thank UAH graduate student Philip Hahn and Mr. John Whyte from Arrow Tech for their help with PRODAS.

TABLE OF CONTENTS

LIST OF FIGURES

LIST OF TABLES

LIST OF SYMBOLS

A_{pin}	Area of fin affected by pin shock (mm^2)
C_l	Roll torque coefficient
$C_{l\delta}$	Roll torque coefficient derivative respect to δ
C_N	Fin normal force coefficient
$C_{N\alpha}$	Fin normal force coefficient derivative
C_Y	Side force coefficient
d	Distance between pin and fin surface (mm)
D	Projectile diameter (mm)
h	Pin height (mm)
L_{fin}	Fin length (mm)
L_p	Distance along the fin affected by pin shock (mm)
L_{cp}	Roll torque moment arm (mm)
M	Mach number
P	Pressure (Pa)
R_c	Bow shock radius of curvature
R	Projectile radius (mm)
r	Pin radius (mm)
t	time (s)
X	Projectile downrange distance (m)
Y_{cp}	Y-component of fin center of pressure (mm)

Y	Projectile lateral displacement (m)
α	Angle of attack (deg)
β	Sideslip angle - positive nose left (deg)
β	Shock angle (deg)
δ	Fin cant/deflection angle (deg)
Δ	Bow shock standoff distance (mm)
η_{sep}	Separation angle between the fin and pin (deg)
φ	Roll angle (deg)
θ	Shock deflection angle (deg)
μ	Mach angle (deg)
γ	Specific heat ratio

CHAPTER I

INTRODUCTION

There has been a surge of interest recently in guided small projectiles operating in the supersonic and hypersonic ranges. According to army missile engineers, a possible scenario would be rapidly shooting these projectiles to intercept incoming rocket, artillery, and mortar (RAM) rounds. The interceptor projectiles must produce large turning forces to achieve high maneuverability and a high hit probability. Historically, movable fins have been used for missile control. However, the volume restrictions of these interceptor projectiles (10 – 40 mm diameter) make packaging an actuator large enough to produce the required turning forces difficult.

A U.S. Army Research Laboratory (ARL) study by Silton [1] has demonstrated that the introduction of control pins in the vicinity of missile fins creates complex shock patterns that impinge on both the fins and body surface. The shock impingements generated by two pins placed diametrically opposed to each other as shown in Figures 1.1 and 1.2 are able to induce a roll moment. These pins could potentially replace moveable control surfaces and larger actuators, which would greatly reduce the complexity and weight of the projectile.

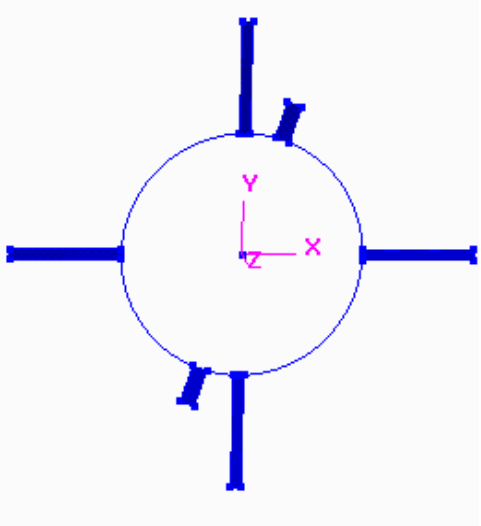

Figure 1.1 Diametrically opposed pin configuration (missile base view)

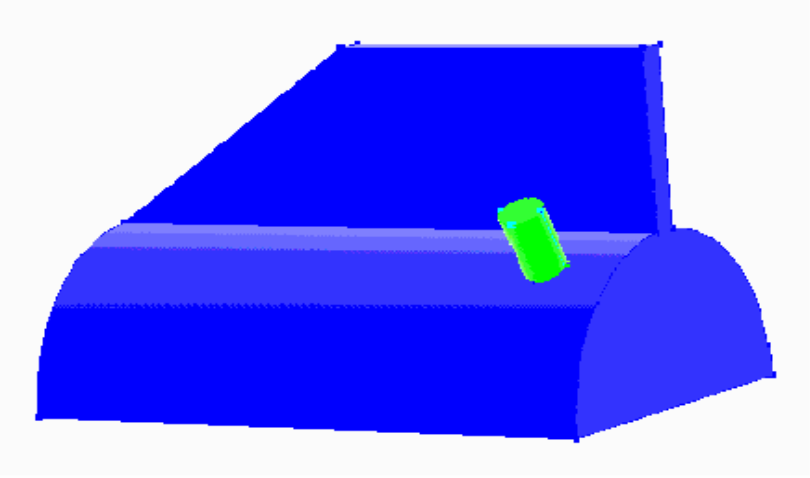

Figure 1.2 Isometric view of diametrically opposed pin in the vicinity of missile fin

The major objective of this thesis was to determine the magnitude of normal force created by opposing pins on the fin surfaces by expanding upon the ARL roll torque results generated by the diametrically opposed pin configuration. Figures 1.3 and 1.4 show how an opposing pin configuration would appear. The normal force acting on the two vertical fin surfaces would theoretically induce a yaw moment on the projectile.

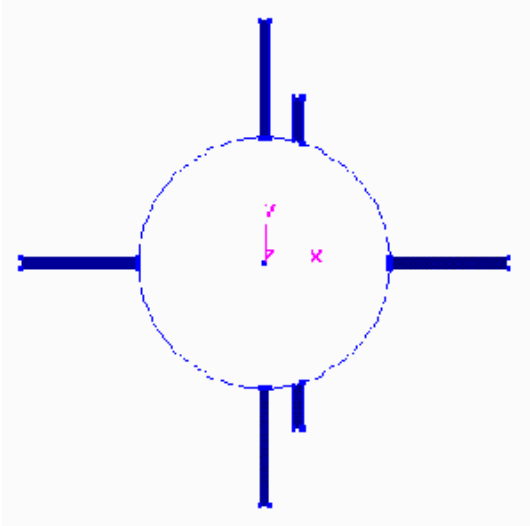

Figure 1.3 Opposing pin configuration (missile base view)

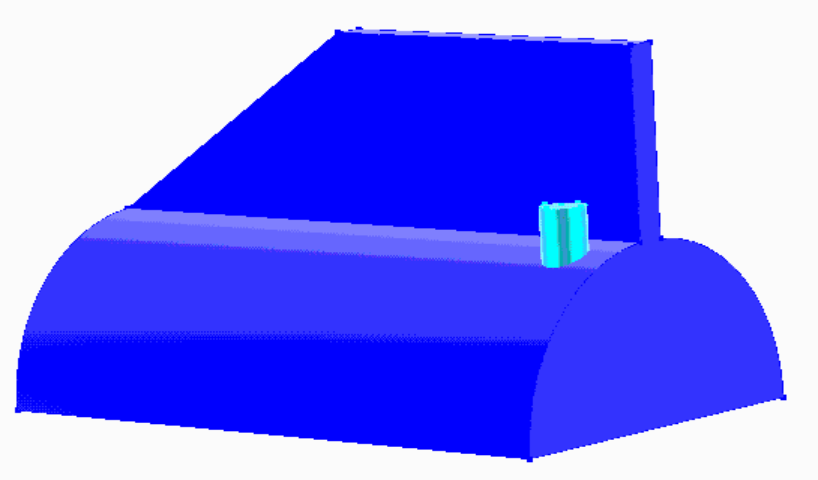

Figure 1.4 Isometric view of opposing pin in the vicinity of missile fin

A simple engineering level Matlab code was written to predict the roll torque and normal force generated through shock impingement for the diametrically opposed pin and the opposing pin configurations. The code was calibrated and verified through comparisons with CFD predictions and data derived from free flight tests in the ARL

spark range [1]. The development of this code could significantly reduce the future cost and effort of full CFD simulations and flight tests.

Variations of pin height, radius, and placement were studied to determine how the configurations affect the roll torque and normal force of a typical projectile. A 6 Degrees-of-Freedom (6-DOF) simulation was used to predict the roll angle as a function of downrange distance for the diametrically opposed pin configuration. For the opposing pin configuration, a controlled trajectory simulation was used to predict the lateral displacement and the sideslip angle as a function of downrange distance. The symmetry of a typical tail control projectile along with an opposing pin configuration for the horizontal fin set shown in Figure 1.5 could also potentially induce a change in angle of attack.

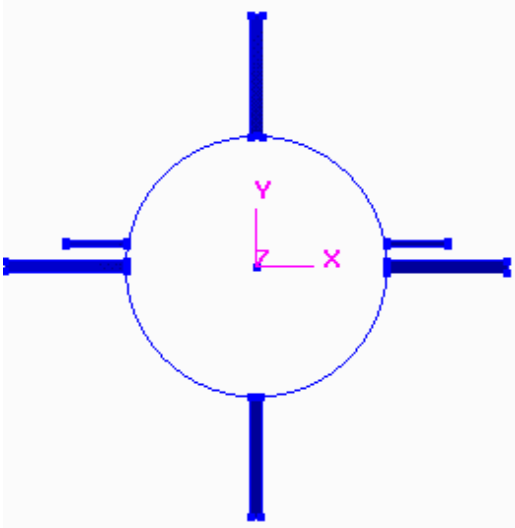

Figure 1.5 Horizontal opposing pin configuration (missile base view)

CHAPTER II

MATLAB ANALYTICAL MODEL

2.1 Overview

The generic projectile [1] studied in this project consists of a tangent ogive nose, cylindrical body, and four fins placed 90 degrees apart from each other. The control system is a tail control. Figure 2.1 shows how the projectile would appear. The exact dimensions of the projectile are listed in Chapter 6.

Figure 2.1 Projectile isometric view (without pins)

A relatively simple two-dimensional semi-empirical model of the control pin aerodynamics was developed and implemented in Matlab. The model strictly focuses on the region where the bow shock generated by the control pin interacts with the fin

surface. Figure 2.2 shows sample output from the model. The pin can be seen as the circle centered at the point (0, 0) with a radius of 0.794 mm (~1/32 in). At a distance of 2.6 mm from the pin, a line is drawn indicating the presence of the fin. The flow is moving from the right to the left. The colored lines shown are the shapes of the bow shocks generated at the corresponding test Mach numbers. Note the shock standoff distance Δ decreases as the Mach number increases.

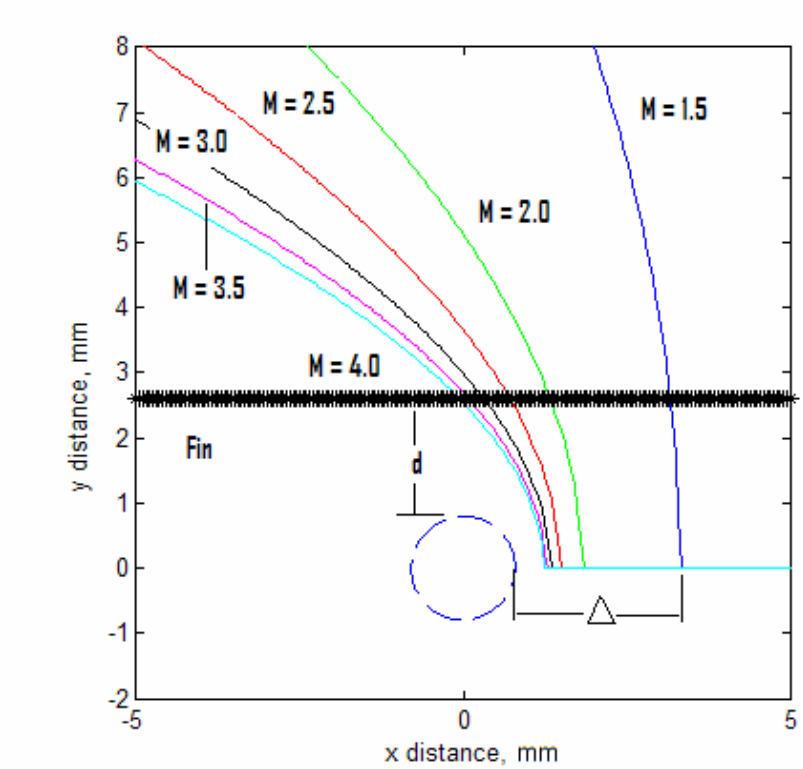

Figure 2.2 Analytical model prediction of cylinder shock shape at various Mach numbers (*r* = 0.794 mm, *d* = 2.6 mm)

2.2 Shock Theory

The flight Mach numbers considered in this study ranged from 1.5 to 4.0. This range is known as the linearized supersonic flow region [2]. Linearized flow problems simplify the analysis because closed-form analytic solutions of the governing equations

are available. Estimation of pressure distributions and resultant aerodynamic forces can be made easily. If the Mach number dips below 1.5 or exceeds 4.0, the projectile will fly in the high transonic or the low hypersonic flow regimes, respectively. In these cases, closed form solutions generally do not exist. Numerical methods would have to be used to solve the systems of nonlinear Navier-Stokes equations.

The control pin in Figure 2.2 is considered to be a cylinder engulfed in a uniform supersonic flow. The exact shape of the bow shock as the flow moves past the cylinder can be described as a function of the freestream Mach number. For Euler (inviscid) flow, the most typical characteristics of the detached shock wave are

- It is normal to the free stream at the stagnation point;
- It is asymptotic to the freestream Mach lines at large distance from the stagnation region.

According to a previous experimental study on supersonic flow around a cylinder by Billig [3], the function that satisfies these requirements is a hyperbola given by

$$\frac{x}{r} = 1 + \frac{\Delta}{r} - \frac{R_c}{r}\cot^2\mu\left[\left(1 + \frac{y^2\tan^2\mu}{{R_c}^2}\right)^{0.5} - 1\right]. \tag{2.1}$$

Here μ is the Mach angle with $\sin\mu = M_1^{-1}$, and r is the radius of the pin. The radius of curvature R_c of the shock wave at the apex of the hyperbola is given by

$$\frac{R_c}{r} = 1.386\exp\left[\frac{1.8}{(M_1 - 1)^{0.75}}\right]. \tag{2.2}$$

The relative shock detachment or standoff distance at the stagnation point is calculated by

$$\frac{\Delta}{r} = 0.386 \exp\left[\frac{4.67}{M_1^{\,2}}\right]. \tag{2.3}$$

The complex interaction of the bow shock with the fin surface produces a mixture of subsonic and supersonic flows. Accurately predicting the pressure distribution on the fin is difficult. This problem was simplified by modeling it as a 2-D supersonic flow with an oblique shock-wall interaction and assuming the shape of the bow shock is linear near the fin surface.

There are three scenarios that could potentially occur as the bow shock interacts with the fin surface [2]. The associated shock structure and flow field Mach numbers are shown in Figures 2.3, 2.4, and 2.6. The following sections describe how the fin pressures are calculated for each case.

Standard Shock Reflection

Figure 2.3 is a schematic of a 2-D oblique shock reflection from a planar surface. As a result of the incident, pin-generated oblique shock, the streamlines in region 2 are inclined at angle θ. As the oblique shock wave interacts with the fin surface, it is deflected at a certain angle and strength as shown in Figure 2.3. The pressure and Mach number (P_2 and M_2) downstream of the incident shock can be determined from the oblique shock relation

$$\frac{P_2}{P_1} = 1 + \frac{2\gamma}{\gamma + 1}(Mn_1{}^2 - 1), \tag{2.4}$$

where $M_{n1} = M_1 \sin\beta$, is the Mach number component normal to the oblique shock. P_1 is the freestream pressure.

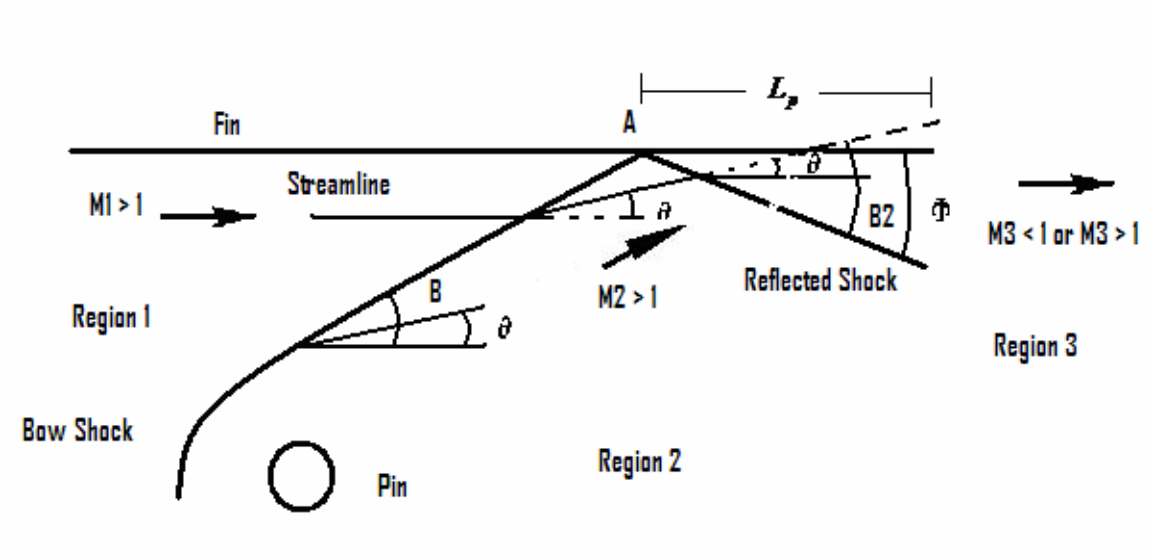

Figure 2.3 Standard shock reflection

In order for the flow to remain parallel to the solid fin surface, another shock wave must be produced at Point A to deflect the flow back by an angle of θ. This second shockwave is called the reflected shock. The final pressure in region 3 is determined by applying a pressure relation similar to Equation (2.4) given by

$$\frac{P_3}{P_2} = 1 + \frac{2\gamma}{\gamma + 1}(Mn_2{}^2 - 1). \tag{2.5}$$

Here, $M_{n2} = M_2 \sin\beta_2$ is the component of M_2 normal to the reflected shock. The reflected shock angle β_2 is determined based on M_2 and θ. Because M_2 is less than M_1, the reflected shock is weaker than the incident shock itself [2]. Note that the angle of the reflected shock to the fin surface is given by

$$\Phi = \beta_2 - \theta . \tag{2.6}$$

In the 2-D model, the bow shock does not curve vertically over the top of the pin. The fin surface area affected by the pin shock has a vertical dimension equal to the pin height and a horizontal dimension equal to L_p. The average pressure acting on this area can be assumed to first-order to be P_3.

Subsonic Reflection

As shown in Figure 2.4, for certain combinations of M_1, pin radius, and fin/pin gap, the flow after the oblique portion of the bow shock is subsonic ($M_2 < 1$). The flow immediately adjacent to the fin becomes parallel to the surface. The average pressure acting on the fin P_2 can be calculated from Equation (2.4).

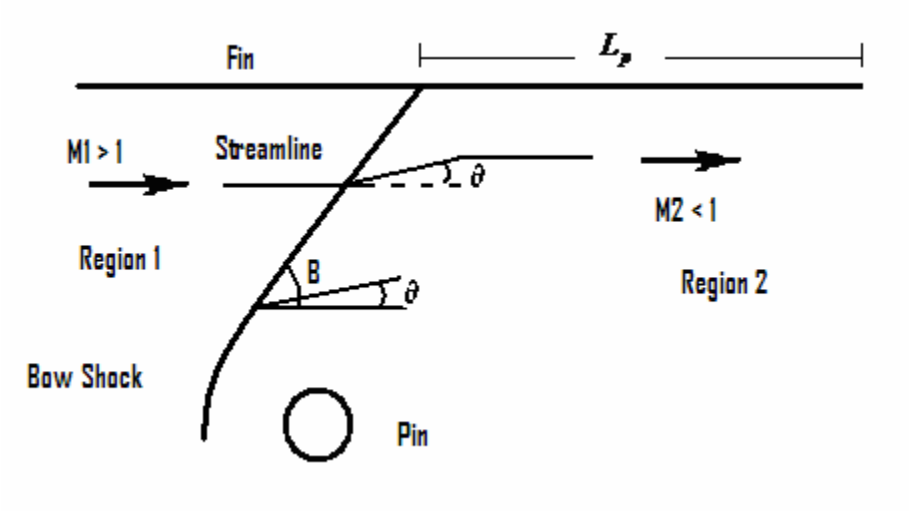

Figure 2.4 Subsonic flow after incident shock

Mach Reflection

Consider the generic θ-β-M plot for M_1 and M_2 shown in Figure 2.5. For the standard shock reflection, the flow deflection due to the incident shock θ_{SR} is less than $\theta_{\max}$ for M_1 and M_2. However, for some flow cases, the deflection required to turn the post bow shock flow back parallel θ_{MR} to the fin exceeds $\theta_{\max}$ for M_2. For these cases, a normal shock is formed to allow the streamlines to flow parallel to the fin as shown in Figure 2.6. The normal shock turns into a curved shock and intersects with the oblique shock further away from the wall. This shock pattern is known as a Mach reflection [2].

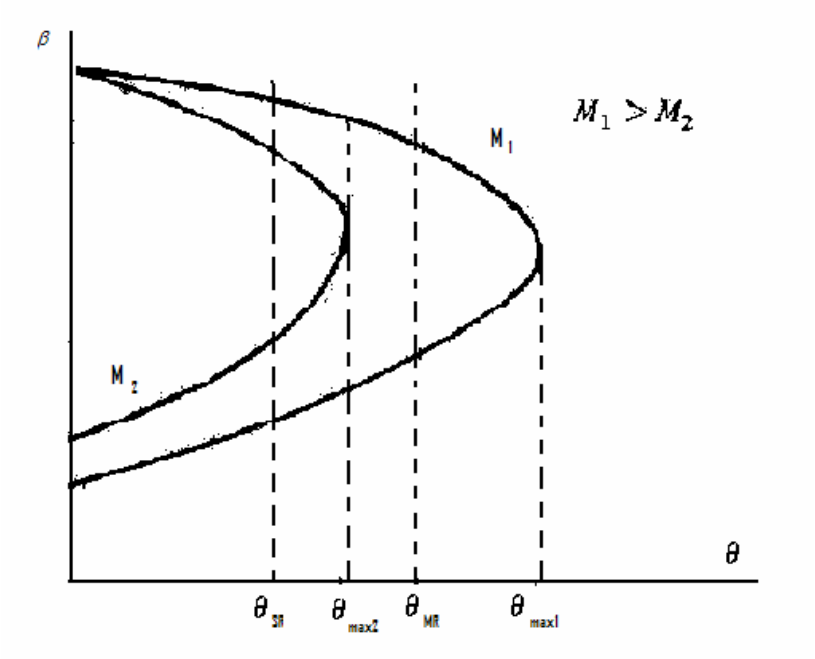

Figure 2.5 *θ-β-M* chart for Mach reflection [2]

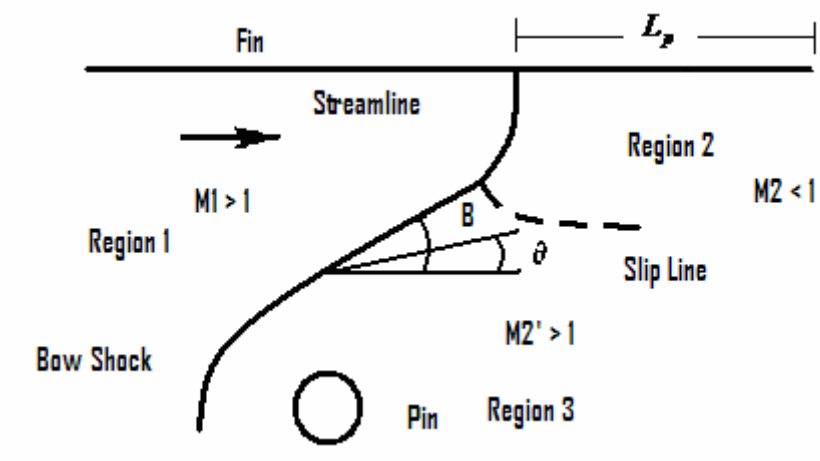

Figure 2.6 Mach reflection

A Mach reflection is inherently hard to model due to the large region of subsonic flow after the normal shock mixing with the supersonic flow after the curved shock. The slip line is a line across which the entropy changes discontinuously between these regions

[2]. Detailed analysis usually requires computational fluid dynamics or other numerical methods.

For the 2-D model, the Mach reflection uses a normal shock pressure relation [2] to determine the pressure acting on the fin surface

$$\frac{P_2}{P_1} = 1 + \frac{2\gamma}{\gamma + 1}(M_1^{\,2} - 1), \tag{2.7}$$

where P_2 is the pressure after the normal shock. This is assumed to be the pressure acting on the fin. It is important to note here that a standard shock reflection often results in a larger final pressure than a Mach reflection, because the two oblique shockwaves offer a stronger compression than a normal shock alone.

2.3 Code Description

A Matlab code (provided in Appendix A) was written to incorporate the various shock reflections described in Section 2.2. The code initially prompts the user to enter values for the freestream pressure and specific heat ratio γ. Next the user enters in values for the projectile nose angle θ_{nose} and fin length. The user then inputs the angular separation between the pin and fin. The separation distance d is calculated from this angle and the projectile radius. Finally, the user enters the distance between pin and projectile base and pin radius r. A schematic of the geometry input parameters is shown in Figure 2.7.

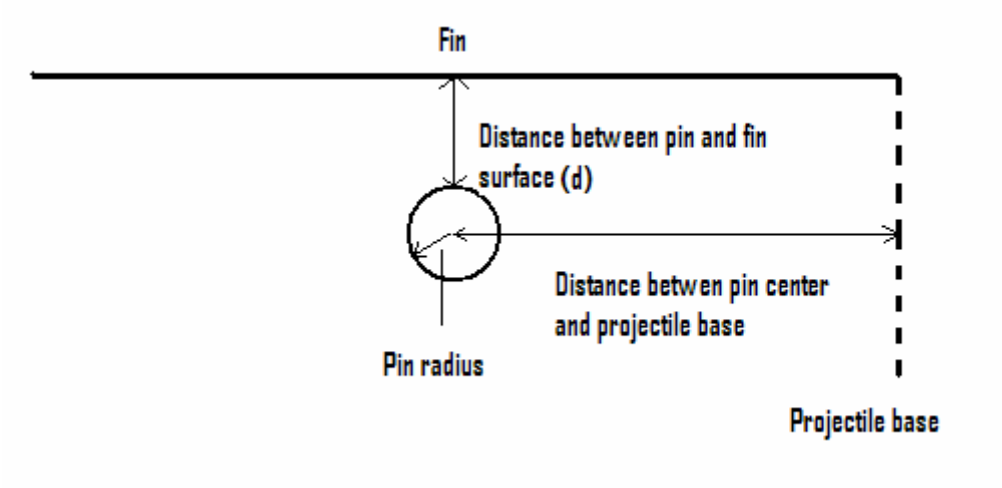

Figure 2.7 Schematic of Matlab pin/fin geometry inputs

The code assumes the projectile nose is a cone and calculates flow properties after the conical nose shock. Figure 2.8 is a 2-D illustration of how the conical shock at the nose would appear. The detailed steps and equations involved can be found in the Matlab code listed in Appendix A. The resultant Mach number and pressure downstream of the conical shock are tabulated in Table 2.1. The nose pressure and Mach number are used as the freestream P_1 and M_1 in the shock-fin reflection calculations.

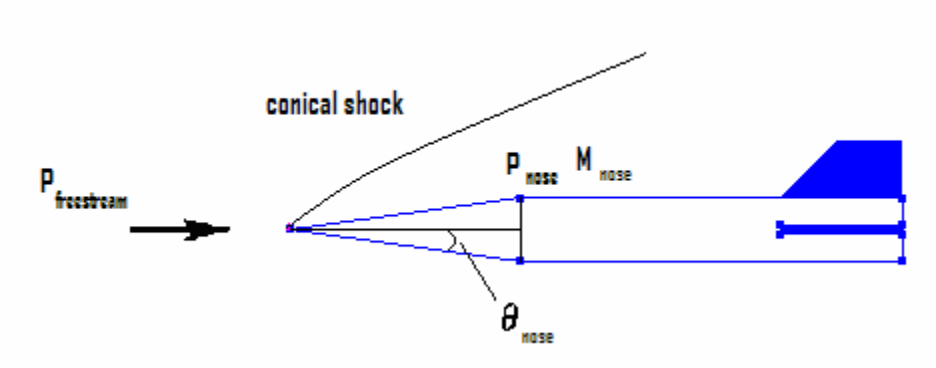

Figure 2.8 2-D Nose shock

Table 2.1 Pressure and Mach number after the conical nose shock (θ_{nose} ~ 7.8 deg)

M (freestream)	*M* (after nose shock)	*P* (freestream) Pa	*P* (after nose shock) Pa
1.50	1.49	101000	101870
2.00	1.97	101000	104580
2.50	2.42	101000	109820
3.00	2.93	101000	113230
3.50	3.36	101000	121000
4.00	3.71	101000	130800

Once again, the pin/fin interaction was modeled as a 2-D cylinder oblique shock-wall interaction problem by assuming the shape of the bow shock is linear in the vicinity of the fin. The Matlab screenshot shown in Figure 2.2 demonstrates that as the Mach number increases, the standoff distance decreases, and the shock lies closer and closer to the pin. The incident shock angle β_1 is determined by using Billig's shock shape function shown in Equation (2.1) to approximate the slope of the shock as it initially interacts with the fin surface as illustrated in Figure 2.9.

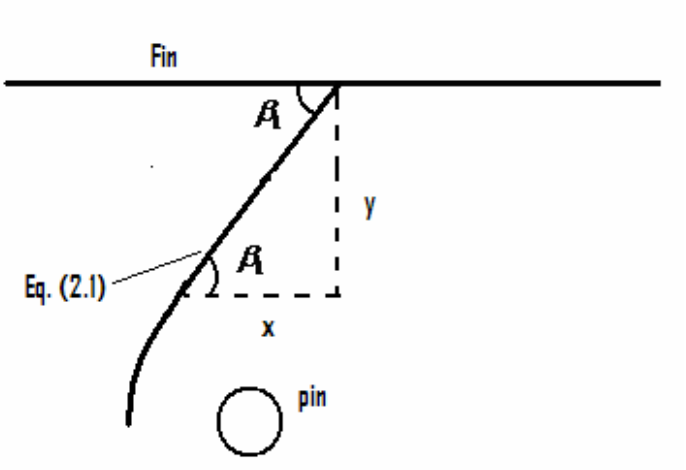

Figure 2.9 Initial shock angle approximation

Once the shock angle β_1 is known, a closed form equation is used to determine the deflection angle θ [2]

$$\theta = \tan^{-1}\left\{\frac{2\cot(\beta)\cdot\left[(M_1{}^2\sin\beta)^2 - 1\right]}{M_1{}^2\cdot\left[\gamma + \cos(2\beta)\right] + 2}\right\}. \tag{2.8}$$

The deflection angles $\theta_{\max 1}$ and $\theta_{\max 2}$ are determined using an exact explicit method [4] given in Appendix B. The type of shock reflection is determined by comparing the value of θ to $\theta_{\max 1}$ and $\theta_{\max 2}$. The Matlab code then calculates the final pressure acting on the fin surface. Again the three scenarios are a standard shock reflection, an oblique shock with a subsonic Mach number after the shock, and a Mach reflection. In the case of a standard shock reflection as shown in Figure 2.3, the same method [4] is used to calculate β_2 for the reflected shock.

The area of the fin surface affected by the reflected shock is approximated by multiplying the pin height by the length along the fin that is disturbed (L_p in Figures 2.3, 2.4, and 2.5). The Matlab code calculates the net force acting on the fin surface by using the pressure calculated in Equations (2.4), (2.5), and (2.6) and subtracting the pressure on the side of the fin away from the pin (~ P_{nose}) from those values. A major assumption implemented in the code is that the final pressure acting on the fin surface after the shock interactions is constant (P_3 in Figure 2.3, P_2 in Figures 2.4 and 2.6). In reality, the flow expands as it moves around the pin, which leads to large regions of low pressure. This is seen later through the pressure contours generated by CFD. The code takes into consideration the discrepancy by averaging the pressure values after the conical nose

shock in Table 2.1 with the final pressures calculated using Equations (2.4), (2.5), and (2.6) for the corresponding Mach numbers. Equation (2.9) shows how Matlab calculates the pin force for a standard shock reflection.

$$F_{pin} = \left[\left(\frac{P_3 + P_{nose}}{2} \right) - P_{nose} \right] \cdot A_{fin} \ . \tag{2.9}$$

The first term $\left(\frac{P_3 + P_{nose}}{2} \right)$ is the average pressure acting on the fin surface nearest the pin. P_{nose} is the pressure on the side away from the pin. A_{fin} is the area of the fin affected by the pin shock.

The Matlab code simplifies the problem down to a 2-D oblique shock-wall interaction. In doing so the curvature of the projectile surface on which the pins are placed is neglected. This can be seen in Figures 2.10 and 2.11. For the roll torque model, the Matlab code should overpredict the pressure exerted by the pin on the fin because it assumes that the distance between the pin and the fin surface is constant (see Figure 2.11). In reality the separation between the fin and pin increases vertically from the projectile surface (see Figure 2.10). This produces a weaker shock that impinges on the fin surface. Therefore, it is apparent that the Matlab code results would become extremely inaccurate if the separation distance between the pin and fin were to increase significantly. To ensure accurate data, the user should keep the angle between the pin and fin surface (η_{sep}) less than 30 degrees.

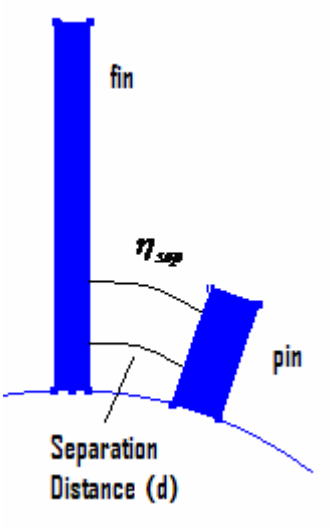

Figure 2.10 Actual pin/fin orientation (not drawn to scale)

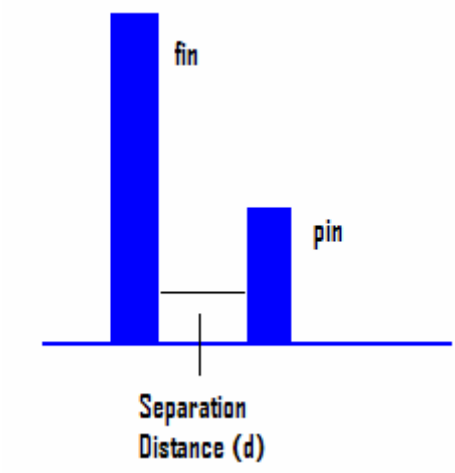

Figure 2.11 Matlab model pin/fin orientation (not drawn to scale)

As shown in Figure 2.12, if the distance between the pin and the projectile base becomes too large, a shock-wall interaction may not physically occur. In this case the results from the Matlab simulation will be meaningless. Therefore, it is best that the user keeps the distance between the pin and projectile base a fraction (< 3/4) of the overall length of the fin (L_{fin}).

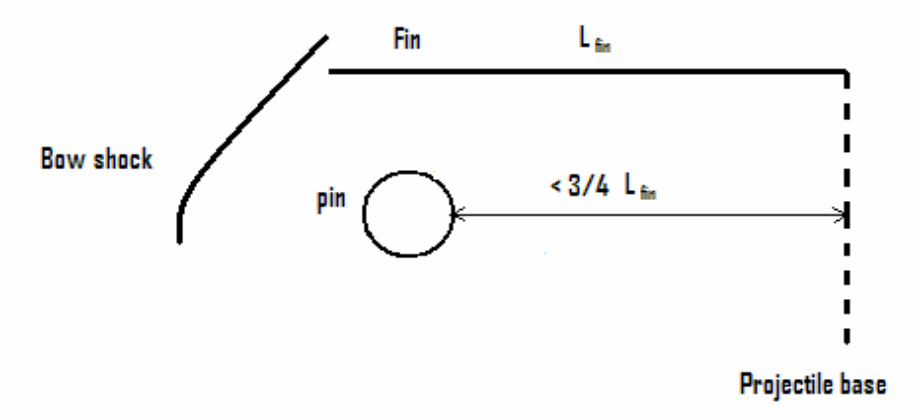

Figure 2.12 No shock-wall interaction scenario

CHAPTER III

MATLAB RESULTS

3.1 Overview

Pins of circular cross-sectional area were used in the analysis. As noted in Chapter I, pin height (1.78 mm and 2.54 mm), radius (0.794 mm ~ 1/32 in and 1.094 mm ~ 1/23 in), and placement with respect to the fin surface (16 deg rotation vs. 24 deg rotation) were studied to determine their effect on the roll torque and normal force coefficients. These choices for pin height, radius, and placement are based on the dimensions from the Silton study [1]. Fully tabulated results from the Matlab simulations are listed in Appendix C.

For the opposing pin model, the normal force coefficient C_N is determined by

$$C_N = \frac{F}{\frac{1}{2}\rho V^2 A}, \tag{3.1}$$

where F is the net pressure force generated by the pins, $\frac{1}{2}\rho V^2$ is the dynamic pressure, and A is the cross-sectional area of the projectile body. This force is determined from Equation (2.9). The term “fin normal force” is used to describe the net force acting on

the fin throughout this paper. However, for the opposing pin configuration, the pin actually generates a side force. The side force coefficient is usually expressed as C_Y.

The roll torque T is defined by the product of the net force acting on the fin F with roll moment arm L_{cp}, where

$$L_{cp} = R + Y_{cp}. \tag{3.2}$$

Here Y_{cp} is the y-component of the fin center of pressure relative to the fin root or body surface, and R is the projectile radius. Figure 3.1 is an illustration of L_{cp} and Y_{cp}. For simplicity purposes, Y_{cp} for the Matlab model was assumed to be half of the pin height.

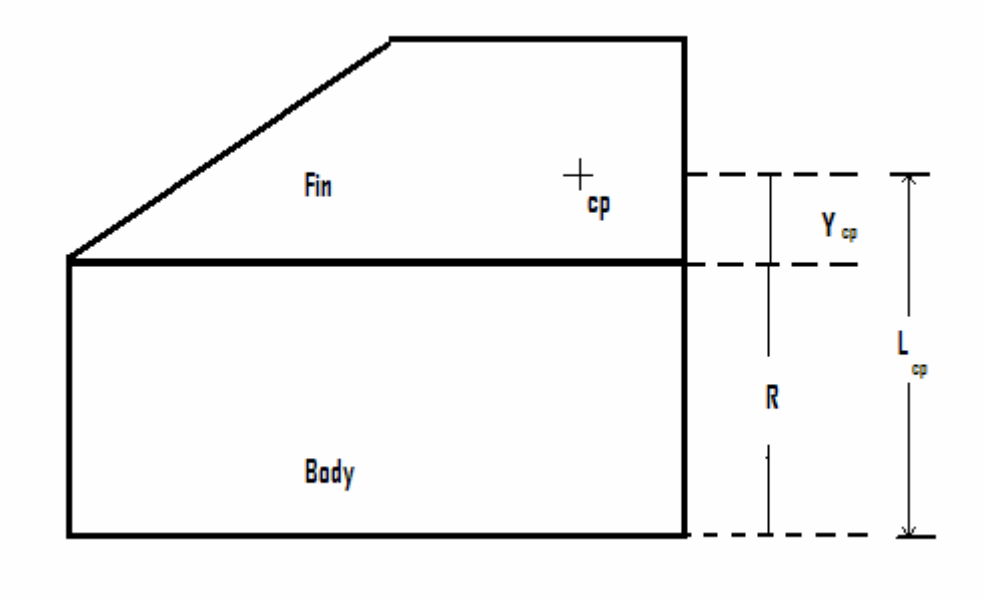

Figure 3.1 Roll torque moment arm definition

The resultant roll torque coefficient C_l is calculated by

$$C_l = \frac{T}{\frac{1}{2}\rho V^2 AD}, \tag{3.3}$$

where D is the projectile diameter.

3.2 Pin Height Variation

Figures 3.2 and 3.3 show that the long pin (2.54 mm height) provided a larger normal force and roll torque as expected. The area of the fin surface affected by the bow shock is obviously more extensive for the long pin model. This is visually demonstrated by the CFD simulations in Chapter 4. Although the coefficients are decreasing with Mach number, the normal force and roll torque are actually increasing with Mach number. This is due to the rapid increase in dynamic pressure as Mach number goes from 1.5 to 4.0. The coefficients also asymptotically approach a constant value after M = 2.5.

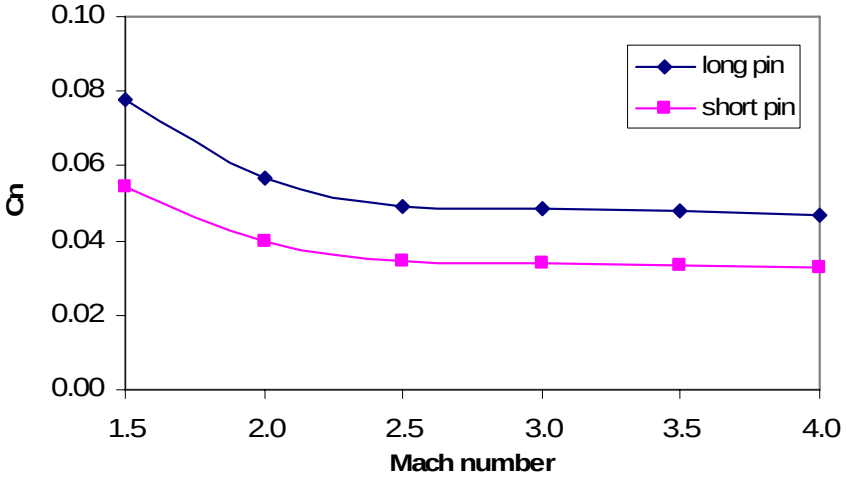

Figure 3.2 Normal force coefficient vs. Mach number (*r* = 0.794 mm, 16 deg pin rotation)

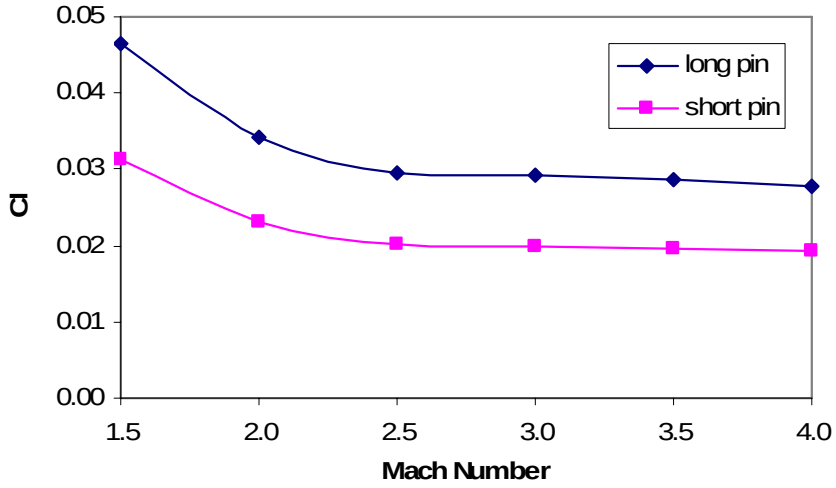

Figure 3.3 Roll torque coefficient vs. Mach number (*r* = 0.794 mm, 16 deg pin rotation)

3.3 Pin Radius Variation

Pins of two different radii (0.794 mm and 1.094mm) were studied. The original hypothesis was that a bigger pin radius would lead to larger normal force and roll torque

values because the bow shock is stronger. As shown in Figures 3.4 and 3.5, this assumption is confirmed for all the Mach numbers except for M = 2.5.

Referring back to Equations (2.1), (2.2), and (2.3), an increase in pin radius leads directly to an increase in shock standoff distance Δ and radius of curvature R_c, which in turn causes the incident shock angle β_1 to increase. Once again, β_1 is determined by estimating the angle at which the incident oblique shock intersects with the fin surface as shown in Figure 2.9. Table 3.1 compares β_1 and the Mach number after the incident shock M_2 for the two pin radii.

Table 3.1 Bow shock incident angle β_1 and post reflection M_2 (h = 2.54 mm, 16 deg pin rotation)

M	r = 0.794 mm, β_1 (deg)	r = 0.794 mm, M_2	r = 1.0794 mm, β_1 (deg)	r = 1.0794 mm, M_2
1.5	83.9	0.54	84.9	0.52
2.0	69.8	0.71	73.2	0.64
2.5	60.3	0.52	64.9	0.87
3.0	52.9	0.48	57.9	0.48
3.5	48.2	0.46	53.7	0.46
4.0	45.7	0.44	51.1	0.44

For the r = 1.0974 mm pin and M = 2.5 case, β_1 was increased such that a subsonic shock reflection occurs (see Figure 2.4). For the M = 2.5 and r = 0.794 mm pin case, a Mach reflection occurs at the fin surface (see Figure 2.6). Since a normal shock is much stronger than an oblique shock, at M = 2.5 the final pressure acting on the fin with r = 0.794 mm (P_2 = 420,000 Pa) is greater than for r = 1.094 mm (P_2 = 350,000 Pa). Figures 3.4 and 3.5 show that a 37 % increase in pin radius leads to the expected increase in normal force and roll torque with an exception of M = 2.5.

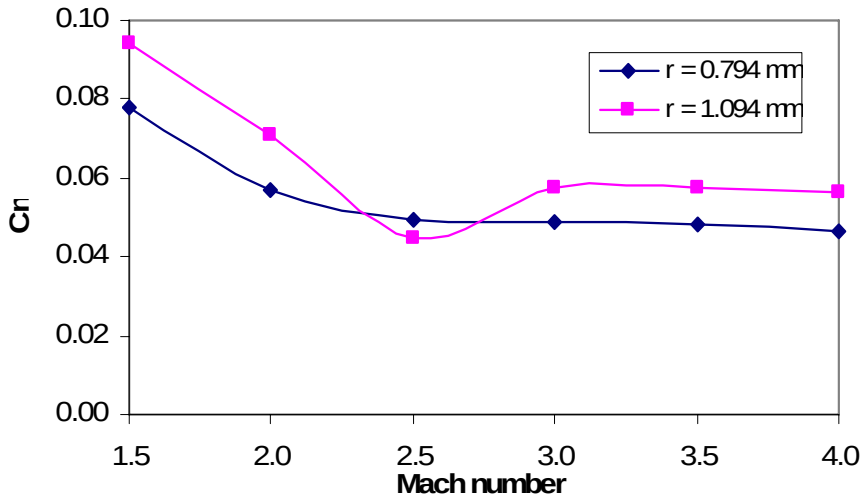

Figure 3.4 Normal force coefficient vs. Mach number (*h* = 2.54 mm, 16 deg pin rotation)

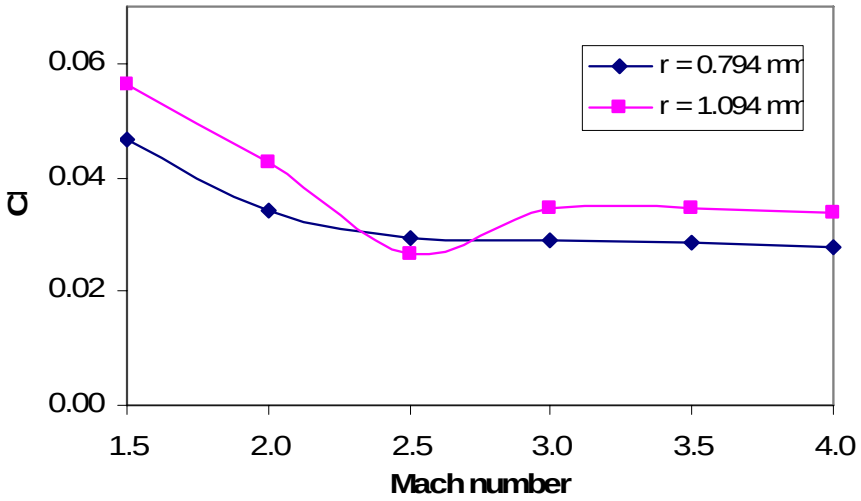

Figure 3.5 Roll torque coefficient vs. Mach number (*h* = 2.54 mm, 16 deg pin rotation)

3.4 Pin Placement With Respect to Fin Surface Variation

Originally the pins were placed at a 16-degree rotation from the fin (η_{sep} in Figure 2.10). An increase in the distance between the pin and the fin surface should

decrease the normal force and roll torque because the shock interacting with the fin surface would be significantly weaker. The simulation data precisely support this claim. Figures 3.6 and 3.7 show that the normal force and roll torque coefficients decrease approximately 5 to 20 percent for the range of Mach numbers as the pin rotation is increased from 16 to 24 degrees with respect to the fin surface.

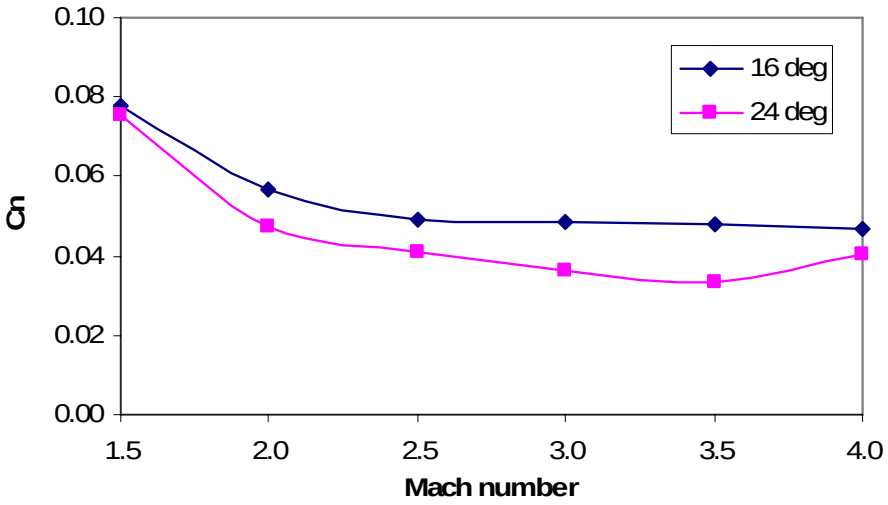

Figure 3.6 Normal force coefficient vs. Mach number
(*h* = 2.54 mm, *r* = 0.794 mm)

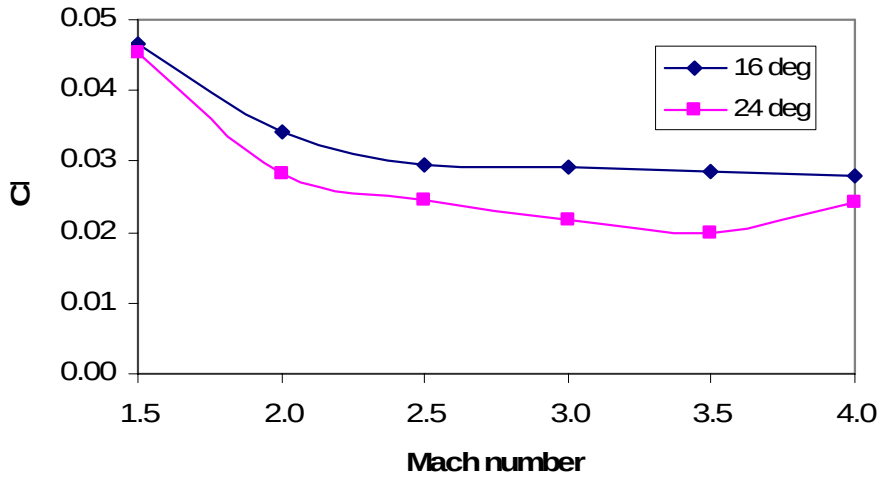

Figure 3.7 Roll torque coefficient vs. Mach number
(*h* = 2.54 mm, *r* = 0.794 mm)

According to Figures 3.6 and 3.7, for the 24 deg model there is a noticeable increase in the normal force and roll torque coefficients between M = 3.5 and M = 4.0. This discrepancy can be attributed to a shock reflection occurring at M = 4.0 as opposed to a Mach reflection for M = 2.5, 3.0, and 3.5. As stated in Section 2.2, in many cases a shock reflection results in a larger final pressure because the two oblique shockwaves can produce a stronger compression than a normal shock alone.

CHAPTER IV

COMPUTATIONAL FLUID DYNAMICS

4.1 Overview

Computational Fluid Dynamics (CFD) simulations were conducted to calibrate and verify the results from the Matlab simulations. Two-dimensional models of the pin/fin configurations were initially created to get a general idea of how the flow would behave at the various Mach numbers. However, due to gridding and other geometric effects these results were only qualitatively used. Three-dimensional models of the pin and fin were created to provide more accurate results. However, due to the lengthy computational time required for the 3-D models, only pin height variation (1.78 mm vs. 2.54 mm) was analyzed with CFD. Pin radius (r = 0.794 mm) and rotation from the fin surface (16 deg) were kept constant. The 3-D simulations strictly model the local fin region using M_{nose} and P_{nose} from Table 2.1 as the inlet Mach number and pressure values.

4.2 Solver

The CFD-Fastran flow solver [5] was utilized to model the various pin/fin combinations. To simplify computation, an inviscid model was used to simulate the two-dimensional cases. Viscous and conductive effects are neglected in the inviscid model;

therefore, the Navier-Stokes equations are reduced to Euler equations. In the three-dimensional simulations, the pointwise k-ϵ turbulence model was used for the computation of the viscous turbulent flow to capture the effects of the shock-boundary layer interactions. The equations were solved within a finite volume framework using a structured grid topology. The point-implicit integration scheme was used to solve the steady-state simulation. For structured grids, Van-Leer's differencing scheme was imposed over its counter part-Roe's scheme-because it is more capable of handling areas of strong gradients [5]. Based on the CFD simulation results from Silton [1], the CFL number was increased to 100 for quicker solution convergence.

4.3 Boundary Conditions

A schematic of the computational domain is shown in Figure 4.1. Unless the boundary is obviously a wall, inlet, or outlet, it was set to pressure, velocity, and temperature-based inflow/outflow conditions. The inflow/outflow condition is used when the user is uncertain of whether the flow will enter or leave the domain at a certain point. The inlet and inflow/outflow properties were set to the M_{nose} and P_{nose} values listed in Table 2.1. An extrapolation outlet boundary condition was set to allow for supersonic outflow. Density was obtained using the perfect gas assumption. On solid surfaces such as the fin and pin, the boundary condition was set to an adiabatic wall [5].

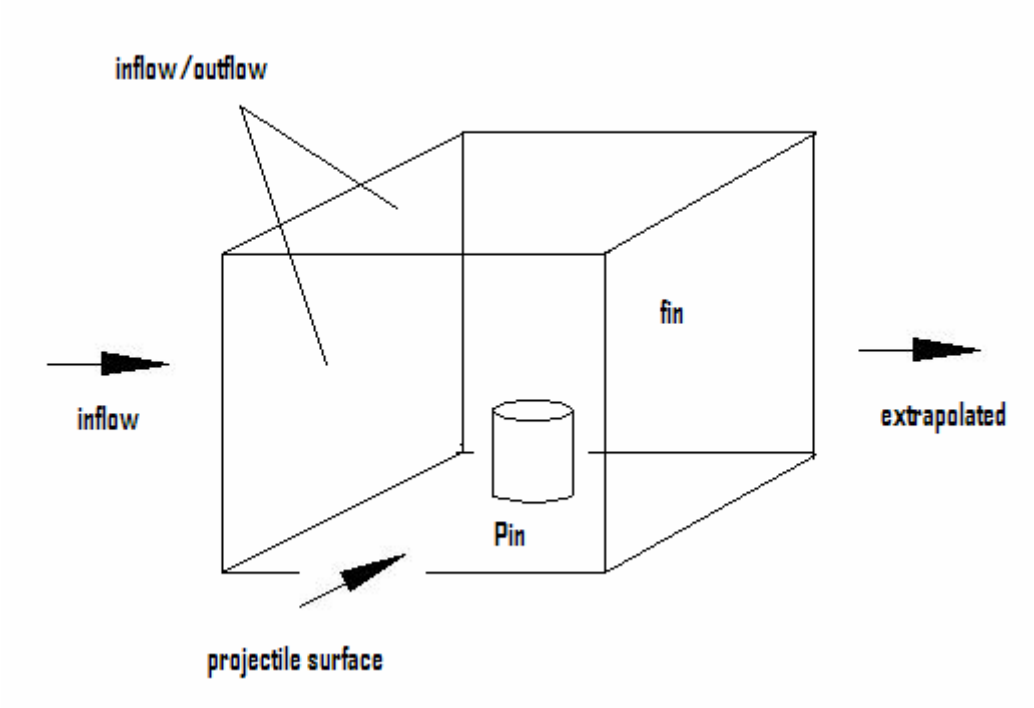

Figure 4.1 3-D computational domain schematic and boundary conditions

4.4 Computational Grid

Structured grids were used for the 2-D and 3-D models because they are easy to deal with in terms of application development, computation, and visualization. Structured grids are built with a repeating geometric and topological structure. One disadvantage associated with structured grids is that they cannot be distorted to increase resolution in a localized region.

Figure 4.2 is an image of the gridding for the 2-D CFD model. The meshes involved in creating the various geometries were fairly coarse, which leads to a decreased accuracy of the results. The calculated shock thicknesses are relatively large due to a coarse grid. However, the main objective of the project was to provide an initial

estimation of the force created by the control pins. The shock thickness was deemed adequate for this purpose.

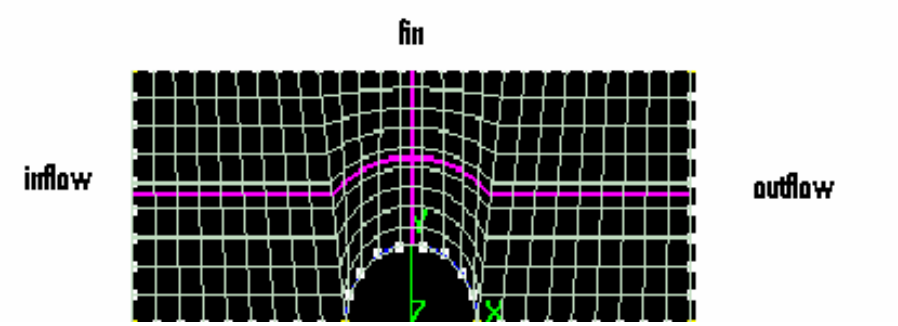

Figure 4.2 2-D CFD model grid (*r* = 0.794 mm, *d* = 2.6 mm)

4.5 2-D Model

CFD-VIEW is a post-processing program implemented by CFDRC to provide easy visualization of CFD flow solver results [6]. In the 2-D CFD generated pressure contours shown in Figures 4.3 and 4.4, red indicates an area of strong pressure and dark blue indicates low-pressure regions. It was expected that the shock structure would resemble the shape described by Billig's model [3] in Equations (2.1), (2.2), and (2.3). However, the results did not support this hypothesis. As the distance between the fin and the pin decreased from 7.5 mm to 2.6 mm, the standoff distance more than doubled. The shape of the shockwave no longer resembled a curved bow shock but appeared more as a normal shock. This phenomenon could be attributed to the lack of a three-dimensional relieving effect. In order to satisfy conservation of mass, the flow has to decelerate through a shockwave as it squeezes past the smaller area between the pin and the fin. Figures 4.3 and 4.4 also suggest that as the distance between the wall and the cylinder

becomes smaller, the shock will form further and further away from the cylinder. Eventually, the shock will lie at the inlet of the computational domain.

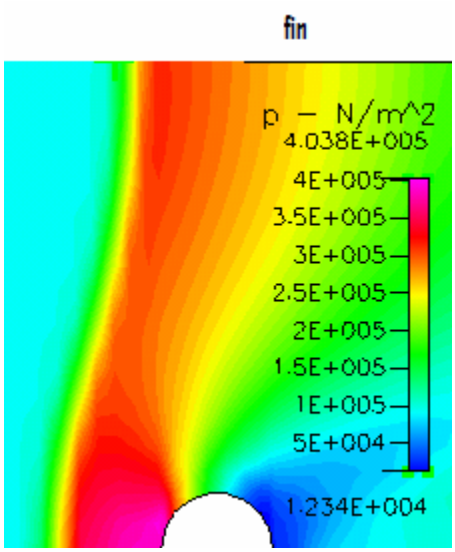

Figure 4.3 Predicted 2-D pressure contours
(*M* = 1.7, *r* = 0.794 mm, *d* = 7.5 mm)

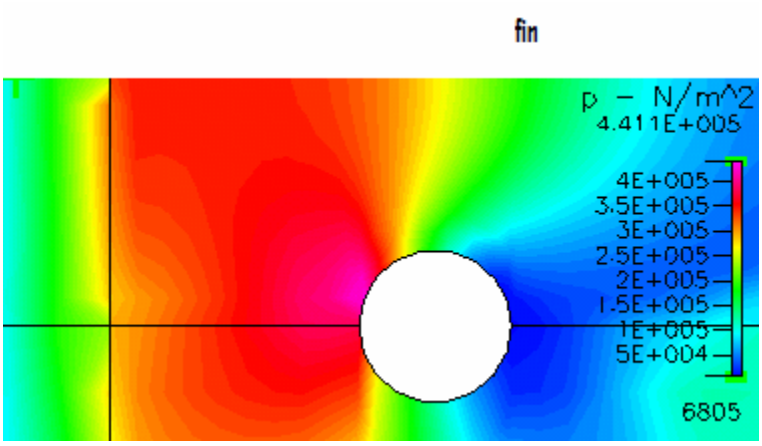

Figure 4.4 Predicted 2-D pressure contours
(*M* = 1.7, *r* = 0.794 mm, *d* = 2.6 mm)

4.6 3-D Model

The 3-D models were generated because they should be more accurate than the 2-D ones. Pin radius (r = 0.794 mm) and rotation from fin surface (16 deg) were kept constant while the pin length was varied between 1.78 mm and 2.54 mm. CFD predictions are tabulated in Appendix D.

As shown in Figures 4.5-4.9, the shock shape predictions with the 3-D model are closer to those predicted by Equations (2.1), (2.2), and (2.3). Unlike the 2-D models, the flow can now escape through the top of the domain. Table 4.1 shows a comparison of the standoff distance between the 3-D CFD simulations and Billig's Equation (2.3). The CFD predicted standoff distance was determined using the CFD-VIEW probe tool. The point where the shock pressure reached approximately 40% of freestream value was used to calculate Δ. The error using CFD ranges from 16 to 24 percent between M = 2.0 and 4.0. Although this is a relatively large percent error, the actual difference in the shock standoff distance between the two methods is miniscule compared to the overall size of the fin surface.

Table 4.1 Standoff distance long pin model (r = 0.794 mm, 16 deg pin rotation)

M	3-D CFD - Standoff Dist (mm)	Billig – Standoff Dist (mm)	Percent Error
1.5	2.500	2.440	2.40
2.0	1.175	0.985	16.17
2.5	0.850	0.647	23.88
3.0	0.650	0.515	20.77
3.5	0.575	0.449	21.91
4.0	0.500	0.410	18.00

In the 3-D CFD model, the standoff distance decreases noticeably as one moves from the bottom to the top of the pin using a probe (see for example Figure 4.5). This

can be explained by the flow trying to gradually merge with the freestream as it moves away from the cylinder in the z-direction. The CFD standoff distance in Table 4.1 is the average value between the top and the bottom of the cylinder. Conversely, Δ values obtained from Equation (2.3) were measured at the pin base.

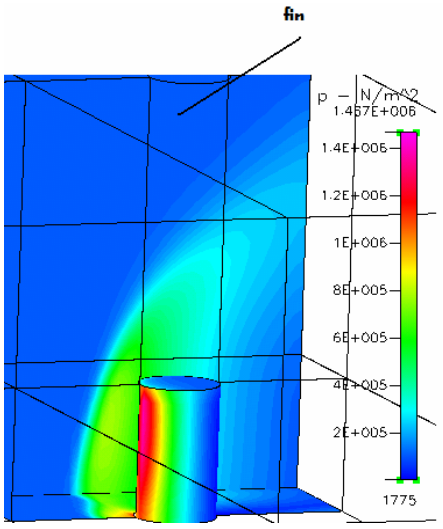

Figure 4.5 3-D CFD simulation isometric view (*M* = 3.0, long pin)

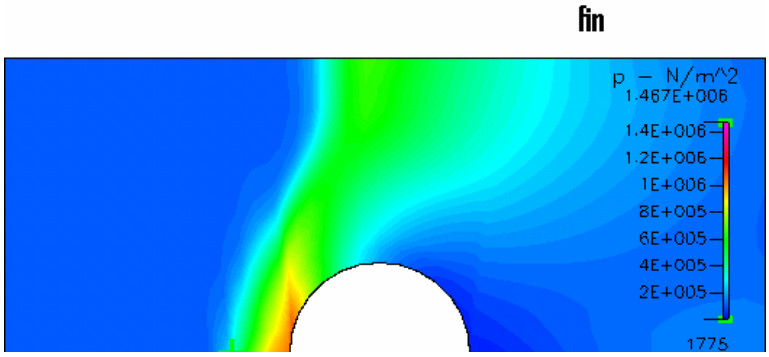

Figure 4.6 3-D CFD simulation top view (*M* = 3.0, long pin)

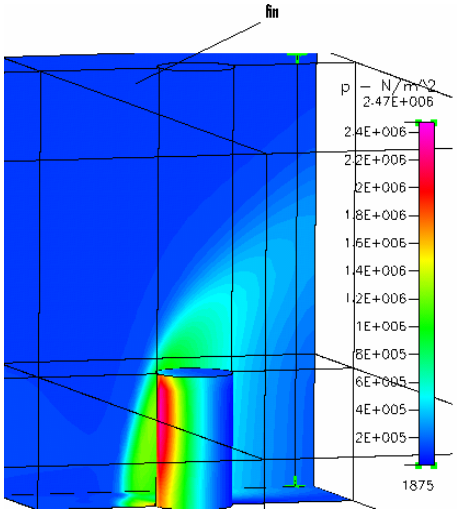

Figure 4.7 3-D CFD simulation isometric view (*M* = 4.0, long pin)

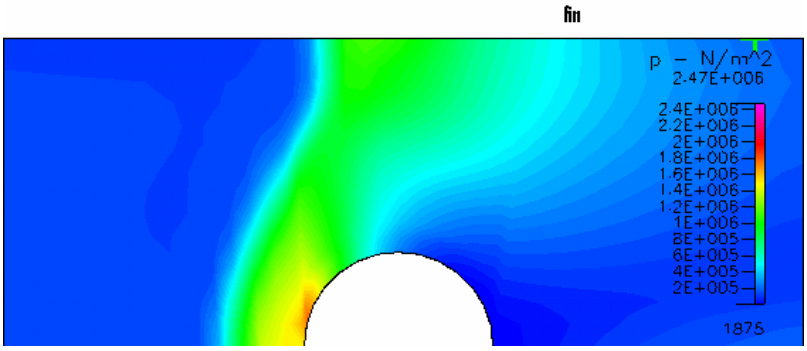

Figure 4.8 3-D CFD simulation top view (*M* = 4.0, long pin)

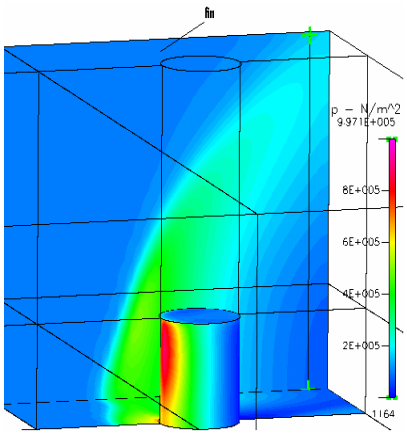

Figure 4.9 3-D CFD simulation isometric view (*M* = 2.5, short pin)

From Figures 4.5-4.9, it is apparent that the pressure acting on the fin surface is much greater at higher Mach numbers. For instance, Figure 4.5 (M = 3.0, long pin) suggests that the maximum pressure acting on the fin surface is approximately 900,000 Pa. As the freestream Mach number increases to 4.0, Figure 4.7 shows a maximum pressure of 1,400,000 Pa. Figures 4.5-4.9 also illustrate that the fin area affected by the bow shock is more extensive at lower Mach numbers.

Similar to the Matlab model, the 3-D CFD models did not take into consideration the curvature of the projectile surface. Once again a flat surface was assumed as shown in Figure 2.11. The separation distance was calculated from the degrees of rotation between the two objects and the radius of the projectile. Assuming a flat projectile surface simplified the geometry creation process greatly; however, the accuracy of the results were somewhat sacrificed. Only an initial approximation of the pin force was desired for this project; therefore, it was reasonable to make this assumption.

4.7 3-D Simulation Results

CFD-VIEW can be used to determine the average pressure and center of pressure on the fin surface. The average pressure acting on the fin was determined by

$$P_{avg} = \frac{\int PdA}{n \cdot dA} \; ; \tag{4.1}$$

here dA is the area of each grid element (a constant) and n is the number of grid elements. As stated in Section 2.3, the net pressure is the difference between the average pressure acting on the fin surface (pin side) and the pressure on the side without the pin. The net

force acting on the fin is then calculated by multiplying the net pressure by the fin surface area.

For the opposing pin configuration shown in Figures 1.3 and 1.4, the normal force is simply equivalent to the total net force acting on the two vertical fin surfaces. The normal force coefficient C_N is calculated by Equation (3.1). The normal force results from the CFD simulations for the long (h = 2.54 mm) and short pin (h = 1.78 mm) models are shown in Tables 4.2 and 4.3. The long pin model produced higher normal force than the short pin as expected.

Table 4.2 CFD prediction of pin normal force (h = 2.54 mm, r = 0.794 mm, 16 deg pin rotation)

***M* (freestream)**	**Net Force (N)**	C_N
1.5	1.48	0.0714
2.0	2.30	0.0623
2.5	3.17	0.0549
3.0	4.18	0.0503
3.5	5.42	0.0479
4.0	6.33	0.0428

Table 4.3 CFD prediction of pin normal force (h = 1.78 mm, r = 0.794 mm, 16 deg pin rotation)

***M* (freestream)**	**Net Force (N)**	C_N
1.5	1.07	0.0515
2.0	1.70	0.0460
2.5	2.32	0.0402
3.0	3.01	0.0362
3.5	3.84	0.0339
4.0	5.30	0.0359

For the diametrically opposed pin configuration shown in Figures 1.1 and 1.2, the roll torque was calculated by multiplying the net force acting on the fin by the roll torque

moment arm L_{cp}. As shown in Equation (3.2), L_{cp} is the sum of the projectile radius *R* and the y-component of the fin center of pressure Y_{cp}. Y_{cp} for the 3-D CFD models was determined by

$$Y_{cp} = \frac{\sum yPdA}{\sum PdA}. \tag{4.2}$$

Here *y* is the vertical distance of each grid element measured from the fin root. Values of L_{cp} at the various Mach numbers for both the long and short pin configurations are tabulated in Table 4.4.

Table 4.4 Roll torque moment arm for 3-D CFD models (*r* = 0.794 mm, 16 deg pin rotation)

***M* (freestream)**	L_{cp} **(m) Long Pin**	L_{cp} **(m) Short Pin**
1.5	0.01077	0.00944
2.0	0.00930	0.00931
2.5	0.00913	0.00916
3.0	0.00901	0.00900
3.5	0.00913	0.00895
4.0	0.00884	0.00869

The roll torque coefficients C_l derived from the CFD predicted pressures for the long (*h* = 2.54 mm) and short (*h* = 1.78 mm) pin models are tabulated in Tables 4.5 and 4.6. Once again the pin radius (*r* = 0.794 mm) and pin rotation from fin (16 deg) were kept constant. As expected, the roll torque increased with pin length because the fin surface area affected by the shock is more extensive for the long pin model. C_l behaves

similarly to C_N because it is assumed in both the Matlab model and CFD simulations that the net force exerted on the fin surface is the same both for the diametrically opposed and opposing pin configurations.

Table 4.5 CFD prediction of roll torque
(*h* = 2.54 mm, *r* = 0.794 mm, 16 deg pin rotation)

***M* (freestream)**	**Net Force (N)**	C_l
1.5	1.48	0.0596
2.0	2.30	0.0449
2.5	3.17	0.0388
3.0	4.18	0.0352
3.5	5.42	0.0339
4.0	6.33	0.0293

Table 4.6 CFD prediction of roll torque
(*h* = 1.78 mm, *r* = 0.794 mm, 16 deg pin rotation)

***M* (freestream)**	**Net Force (N)**	C_l
1.5	1.07	0.0377
2.0	1.70	0.0332
2.5	2.32	0.0286
3.0	3.01	0.0252
3.5	3.84	0.0236
4.0	5.30	0.0241

CHAPTER V

MATLAB AND CFD SIMULATION COMPARISONS

Results obtained from the simple Matlab model were compared to the 3-D CFD simulations for the different pin/fin geometries described in Section 4.1. The Matlab model and CFD predicted roll torque coefficients for the short pin model were then compared to the ARL spark range test data [1].

5.1 Opposing Pins - Normal Force Coefficient

As shown in Figure 5.1 and Table 5.1, the Matlab model predictions are in good agreement with the CFD results in predicting the normal force. The normal force is also the side force depending on the pin locations as stated in Section 3.1. The CFD code predicts an almost linearly decreasing coefficient with Mach number. The Matlab code predicts an almost exponentially decreasing trend with the coefficient approaching a constant value at Mach 4.0.

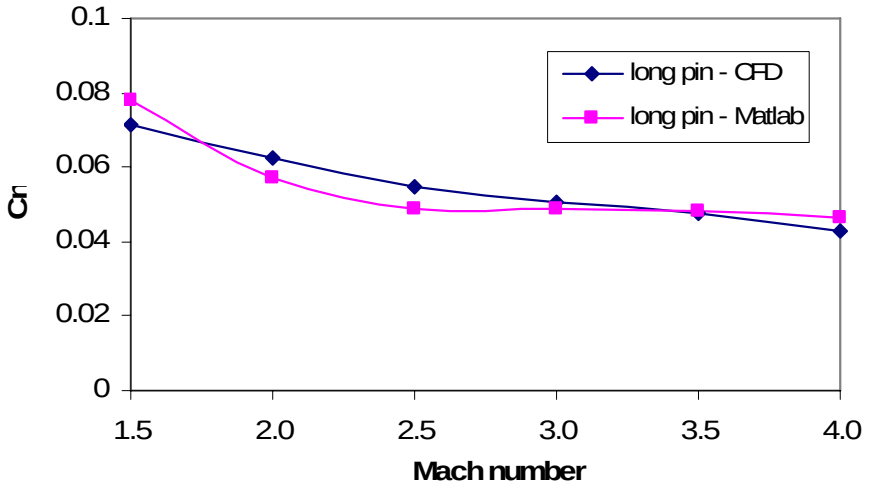

Figure 5.1 Normal force coefficient vs. Mach number (*r* = 0.794 mm, 16 deg pin rotation)

Table 5.1 Normal force coefficient vs. Mach number (long pin, *r* = 0.794 mm, 16 deg pin rotation)

M (freestream)	C_n (CFD)	C_n (Matlab)	Percent Difference
1.5	0.0714	0.0778	8.96
2.0	0.0623	0.0570	-8.51
2.5	0.0549	0.0491	-10.56
3.0	0.0503	0.0487	-3.18
3.5	0.0479	0.0480	0.21
4.0	0.0428	0.0467	9.11

5.2 Diametrically Opposed Pins - Roll Torque Coefficient

As shown in Figure 5.2 and Table 5.2, the Matlab code consistently underpredicted the roll moment compared to the CFD results. However, the discrepancies between the two sets of data are no more than 25 percent for the given Mach numbers. The largest differences are for the lower Mach numbers. The CFD model suggests a slight nonlinear relationship between C_l and Mach number, whereas the Matlab code predicts more of an exponential decay trend. The Matlab predicted roll

torque coefficients are almost constant after M = 2.5. Nonetheless, the relatively simple 2-D Matlab model provided reasonably accurate results. This accuracy is acceptable considering problem complexity and the numerous assumptions that were involved. It will be shown that the Matlab predictions are actually better representations of flight data than the CFD values.

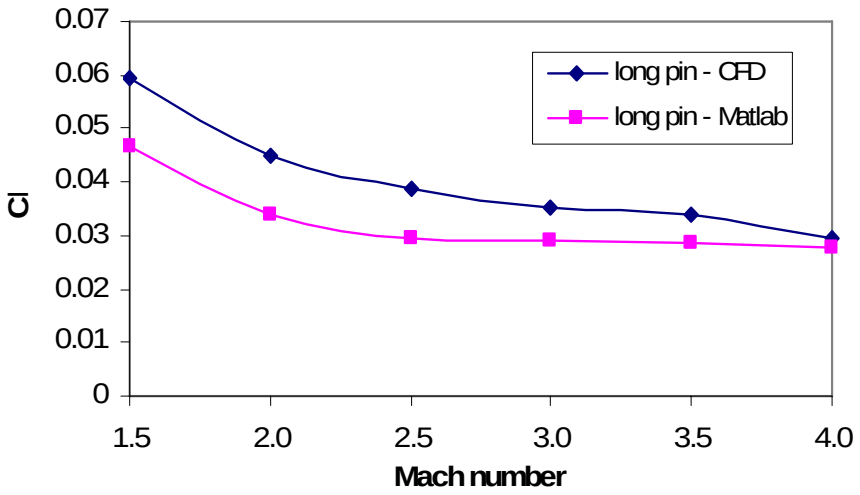

Figure 5.2 Roll torque coefficient vs. Mach number (r = 0.794 mm, 16 deg pin rotation)

Table 5.2 Roll torque coefficient vs. Mach number (long pin, r = 0.794 mm, 16 deg pin rotation)

M (freestream)	C_l (CFD)	C_l (Matlab)	Percent Difference
1.5	0.0596	0.0466	-21.81
2.0	0.0449	0.0341	-24.05
2.5	0.0388	0.0294	-24.23
3.0	0.0352	0.0291	-17.33
3.5	0.0339	0.0287	-15.34
4.0	0.0293	0.0279	-4.78

5.3 Comparison to Flight Test Data

In Silton's AIAA paper [1] roll torque coefficients were obtained from spark range tests for the short pin model at Mach numbers of 2.0, 2.5, and 3.0. The projectile was fired, using EXPRO propellant, from a modified 25 mm Bushmaster Mann barrel [1]. The ARL range facility consists of 39 orthogonal spark shadowgraph stations arranged in 5 groups over 100 m of trajectory length. The first station is located approximately 4.57 m downrange of the muzzle. Infared sensors detect the passage of the projectile and a computer system triggers the spark sources that project a vertical and horizontal direct shadow image of the passing projectile on 29.9 x 25.6 cm film. The stations are surveyed into a fiducial system that is simultaneously imaged on the film with the projectile. The film is processed after each shot and read using a precision light table to produce the raw experimental data. These data include the measured spatial coordinates (range, deflection, altitude) and the angular orientation (pitch, yaw, roll) relative to the earth fixed range coordinate system, all as a function of the spark time. Schematics and photos of the spark range are provided in Silton's report [1].

Roll torque results from the CFD and Matlab simulations are compared with the range test data in Figure 5.3. The range test points (in blue) are the average values of the three shots fired at each Mach number. It is assumed that the spark range data is the standard. Matlab predicted C_l with $Y_{cp} = h/2$, CFD predicted C_l with Y_{cp} calculated from Equation (4.2), and CFD predicted C_l with $Y_{cp} = h/2$, which are indicated by the pink, dark blue, and red markers respectively in Figure 5.3.

Matlab slightly overpredicted C_l at Mach 2.0 and 2.5 but closely correctly predicted the value at Mach 3.0. CFD overpredicted the roll torque coefficient at each of the Mach numbers. At Mach 2.0 and 2.5, CFD (assuming $Y_{cp} = h/2$) overpredicted the flight test data by 19% and 23% respectively. At Mach 3.0, it almost correctly predicted the flight test value.

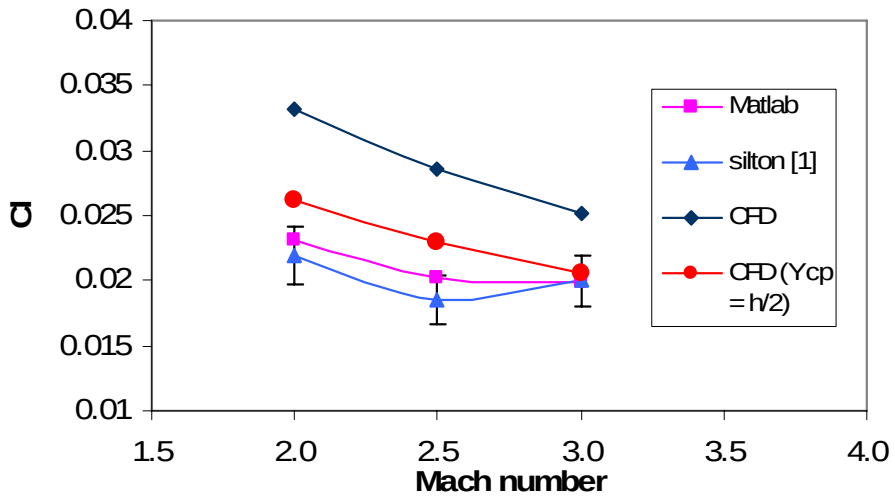

Figure 5.3 Roll torque coefficient vs. Mach number (Short pin, *r* = 0.794 mm, 16 deg pin rotation)

Table 5.3 shows the numerical comparisons between the four sets of data. Similar to the Matlab model, the flight test C_l decreases from Mach 2.0 to 2.5 and then increases slightly at Mach 3.0. The discrepancy between the two sets of data might be caused by a non-zero angle-of-attack during the flight tests [1]. It is important to note that even a 10 percent uncertainty in the experimental data (indicated by bars on the flight test data) can more than account for this difference. It was stated in Section 4.5 that the fin area

affected by the pin shock decreases with increasing Mach number. At higher Mach numbers, the actual fin area affected by the shock becomes closer to the Matlab assumption. This may explain the similarity of the C_l values at Mach 3.0 between the Matlab and flight test data.

Table 5.3 Matlab & CFD vs. flight test (short pin configuration)

M	C_l (Matlab)	C_l (CFD)	C_l CFD ($Y_{cp} = h/2$)	C_l (Silton)	Matlab % Error	CFD % Error	CFD ($Y_{cp} = h/2$) % Error
2.00	0.02	0.03	0.03	0.02	5.00	50.91	19.09
2.50	0.02	0.03	0.02	0.02	9.19	54.59	23.78
3.00	0.02	0.03	0.02	0.02	-0.50	26.00	3.00

CFD shows an almost linear decrease in roll coefficient with Mach number while overpredicting the flight test data by 54% (M = 2.5) to 26% (M = 3.0). The major factor that may account for this drastic difference between the two sets of data is that the 3-D CFD models did not take into consideration the curvature of the projectile surface. As shown in Figures 2.10 and 2.11, in reality the separation between the fin and the pin increases vertically causing the strength of the shock that impinges on the fin surface to diminish. It is apparent that assuming a flat projectile surface results in higher-than-expected pin force values. Grid resolution may also have contributed to this discrepancy.

The Matlab model also assumed a flat surface; however, it compensated for this in other ways. Figures 5.4 and 5.5 illustrate how the Matlab code assumes the area of the fin affected by the shock (A_{pin}) has the height of the pin. In addition, the Matlab model assumes the roll torque moment arm Y_{cp} to be half of the pin height. These assumptions

counteract the pressure overprediction which explains the remarkable resemblance between the Matlab model and the flight test data.

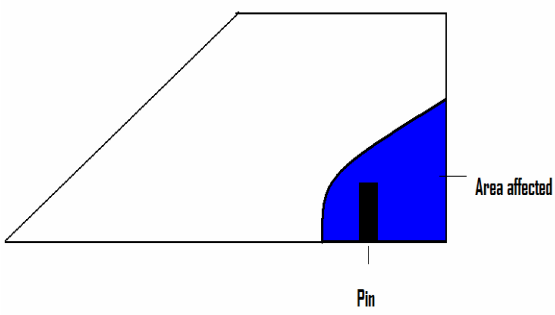

Figure 5.4 Actual A_{pin}

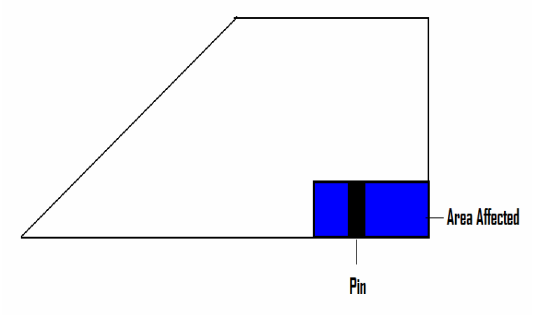

Figure 5.5 Matlab assumption for A_{pin}

CHAPTER VI

TRAJECTORY SIMULATIONS

6.1 Overview

Simulations were performed using the PRODAS code [7] to determine the roll and yaw performance of a pin guided projectile as it travels down a 100 m aeroballistic range. PRODAS is an engineering level code that allows the user to create a projectile model, calculate its mass properties, predict a full set of aerodynamic coefficients, and simulate a test firing. A 6 degrees-of-freedom (6-DOF) trajectory simulation was implemented for the diametrically opposed pin model. The trajectory simulation implemented for the opposing pin model used the CONTRAJ option. CONTRAJ is similar to the 6-DOF model except it allows the user to manually specify an effective fin deflection angle δ (also know as the control angle) at a certain time to simulate the pin control force that is acting on the fin surface. Numerical integration of the equations of motion is accomplished with a fourth order Runge-Kutta integrator [7]. Both trajectory simulations predicted the roll, pitch, yaw angles and rates along with other parameters as a function of downrange distance.

6.2 Projectile Dimensions and Initial Analysis

Figure 2.1 shows a model of the projectile created in PRODAS. Figure 6.1 shows the top and base views of the projectile. The exact dimensions and materials are similar to the configuration studied by Silton [1]. The geometry consists of a 46.0 mm tangent ogive nose with a blunt nose tip radius of 0.635 mm, a 56.9 mm long body, and a 22.4 mm long tail. For stability, the center-of-gravity was shifted forward by utilizing tungsten for the nose and hollowed out aluminum for the body and fins [1]. The projectile body radius is approximately 6.45 mm. Each individual fin is 1.02 mm thick with a 25.75-degree sweep angle, a 22.4 mm root chord, and a 10.4 mm tip chord. The overall fin span is 25 mm [1].

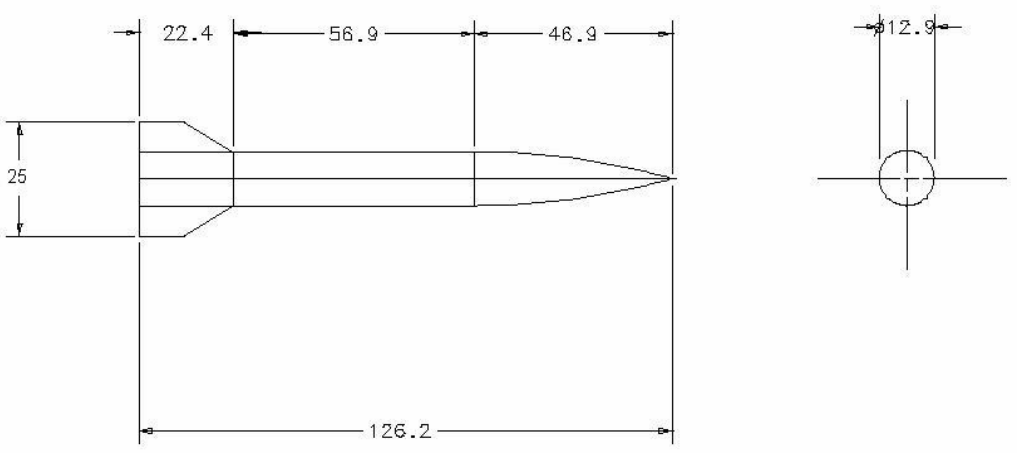

Figure 6.1 Projectile top and base views (without pins)

Figure 6.2 shows the mass properties of the projectile calculated by PRODAS before and after launch. The model has a mass of 117 grams and its center of gravity is located 53.3 mm from the nose. The axial and transverse moments of inertias are 21.6

and 885.4 $gm \cdot cm^2$. These values remain constant during the trajectory because the projectile is not carrying any propellant. Figure 6.3 shows the PRODAS stability analysis screen for the projectile at M = 4.0 (~1364.0 m/sec). The center of pressure is located 66.3 mm behind the nose. The static margin is approximately 1 caliber – indicating that the projectile is longitudinally stable.

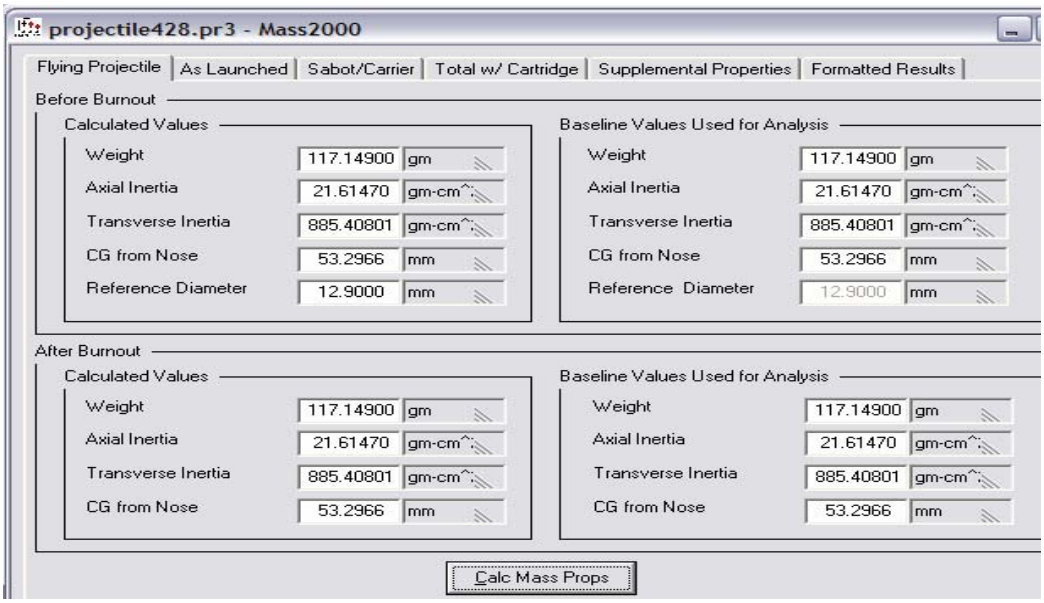

Figure 6.2 PRODAS projectile mass properties screen

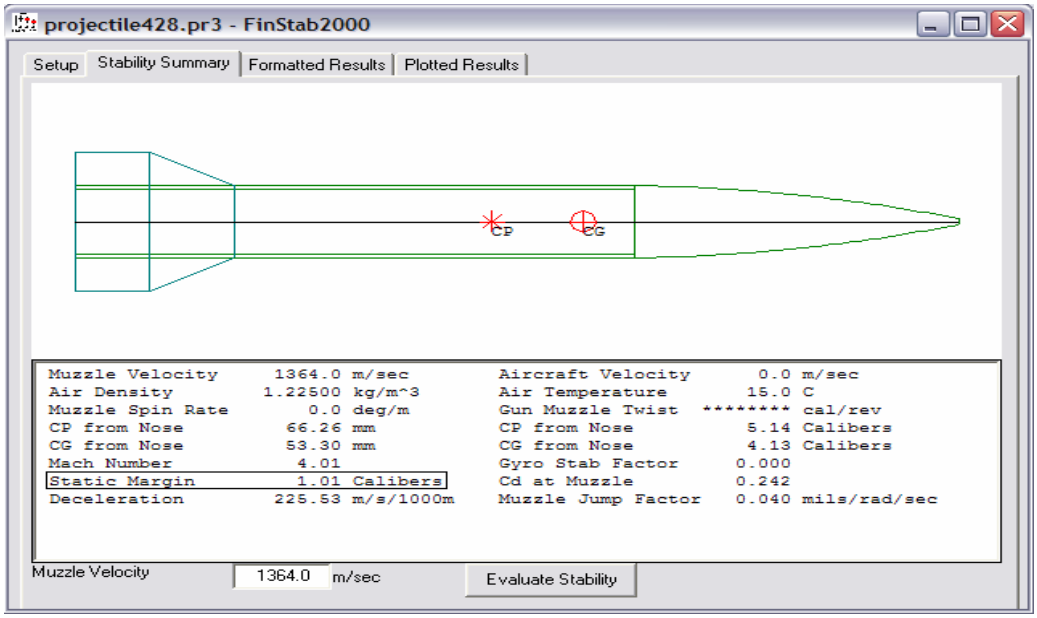

Figure 6.3 PRODAS projectile stability analysis screen

6.3 Initial Conditions

The launch gun for all simulations is assumed to have an elevation of 0.001 deg and zero azimuth. Standard sea level conditions are used for the temperature and pressure. The gun twist, or the distance it takes the projectile to rotate 360 deg, was set to 10,000 in order to insure that the initial angular velocity is essentially zero. The initial velocity was set to the corresponding test Mach number. Finally, the initial yaw and pitch angles along with the pitch rates were set to zero. Figure 6.4 is a PRODAS screenshot of the initial condition page in 6-DOF.

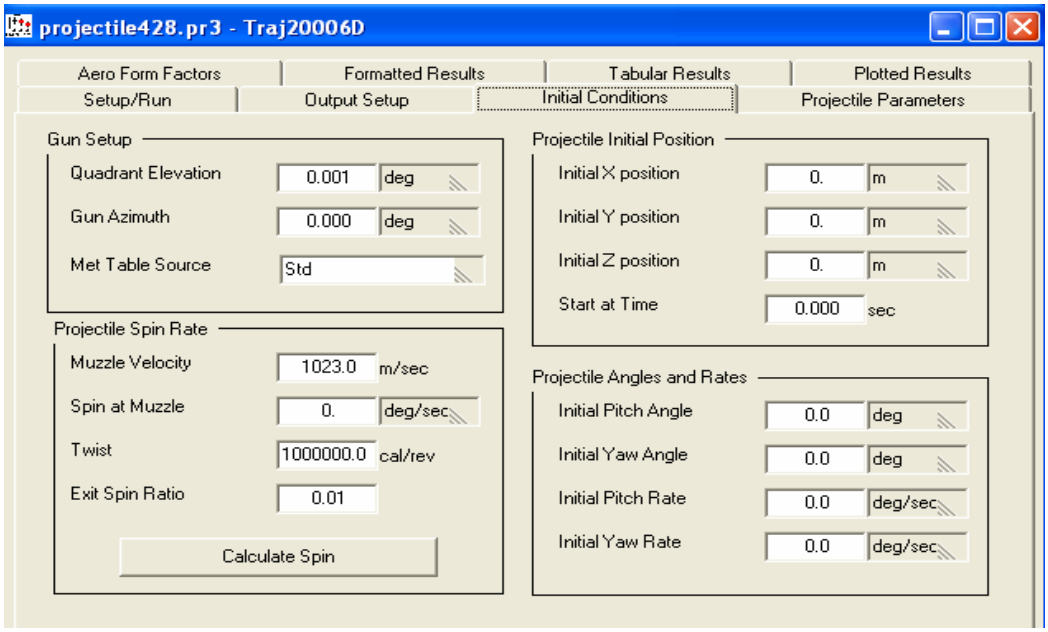

Figure 6.4 PRODAS 6-DOF initial condition screen

6.4 Diametrically Opposed Pins – Roll Performance

PRODAS generates a database of aerodynamic coefficients as a function of Mach number using the spinner (spin stabilizing munitions), finner (finned projectiles), or AP98 model [7]. These coefficients are for a projectile without control pins. Figure 6.5 is a screenshot of the PRODAS aerodynamics look up table for the finner data base.

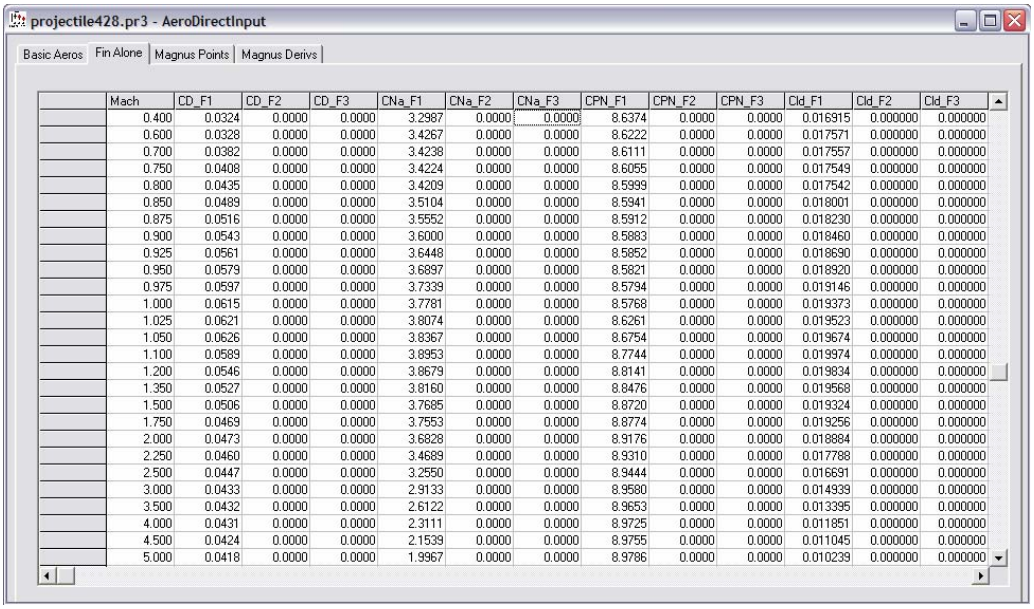

Mach	CD_F1	CD_F2	CD_F3	CNa_F1	CNa_F2	CNa_F3	CPN_F1	CPN_F2	CPN_F3	Cld_F1	Cld_F2	Cld_F3
0.400	0.0324	0.0000	0.0000	3.2987	0.0000	0.0000	8.6374	0.0000	0.0000	0.016915	0.000000	0.000000
0.600	0.0328	0.0000	0.0000	3.4267	0.0000	0.0000	8.6222	0.0000	0.0000	0.017571	0.000000	0.000000
0.700	0.0382	0.0000	0.0000	3.4238	0.0000	0.0000	8.6111	0.0000	0.0000	0.017557	0.000000	0.000000
0.750	0.0408	0.0000	0.0000	3.4224	0.0000	0.0000	8.6055	0.0000	0.0000	0.017549	0.000000	0.000000
0.800	0.0435	0.0000	0.0000	3.4209	0.0000	0.0000	8.5999	0.0000	0.0000	0.017542	0.000000	0.000000
0.850	0.0489	0.0000	0.0000	3.5104	0.0000	0.0000	8.5941	0.0000	0.0000	0.018001	0.000000	0.000000
0.875	0.0516	0.0000	0.0000	3.5552	0.0000	0.0000	8.5912	0.0000	0.0000	0.018230	0.000000	0.000000
0.900	0.0543	0.0000	0.0000	3.6000	0.0000	0.0000	8.5883	0.0000	0.0000	0.018460	0.000000	0.000000
0.925	0.0561	0.0000	0.0000	3.6448	0.0000	0.0000	8.5852	0.0000	0.0000	0.018690	0.000000	0.000000
0.950	0.0579	0.0000	0.0000	3.6897	0.0000	0.0000	8.5821	0.0000	0.0000	0.018920	0.000000	0.000000
0.975	0.0597	0.0000	0.0000	3.7339	0.0000	0.0000	8.5794	0.0000	0.0000	0.019146	0.000000	0.000000
1.000	0.0615	0.0000	0.0000	3.7781	0.0000	0.0000	8.5768	0.0000	0.0000	0.019373	0.000000	0.000000
1.025	0.0621	0.0000	0.0000	3.8074	0.0000	0.0000	8.6261	0.0000	0.0000	0.019523	0.000000	0.000000
1.050	0.0626	0.0000	0.0000	3.8367	0.0000	0.0000	8.6754	0.0000	0.0000	0.019674	0.000000	0.000000
1.100	0.0589	0.0000	0.0000	3.8953	0.0000	0.0000	8.7744	0.0000	0.0000	0.019974	0.000000	0.000000
1.200	0.0546	0.0000	0.0000	3.8679	0.0000	0.0000	8.8141	0.0000	0.0000	0.019834	0.000000	0.000000
1.350	0.0527	0.0000	0.0000	3.8160	0.0000	0.0000	8.8476	0.0000	0.0000	0.019568	0.000000	0.000000
1.500	0.0506	0.0000	0.0000	3.7685	0.0000	0.0000	8.8720	0.0000	0.0000	0.019324	0.000000	0.000000
1.750	0.0469	0.0000	0.0000	3.7553	0.0000	0.0000	8.8774	0.0000	0.0000	0.019256	0.000000	0.000000
2.000	0.0473	0.0000	0.0000	3.6828	0.0000	0.0000	8.9176	0.0000	0.0000	0.018884	0.000000	0.000000
2.250	0.0460	0.0000	0.0000	3.4689	0.0000	0.0000	8.9310	0.0000	0.0000	0.017788	0.000000	0.000000
2.500	0.0447	0.0000	0.0000	3.2550	0.0000	0.0000	8.9444	0.0000	0.0000	0.016691	0.000000	0.000000
3.000	0.0433	0.0000	0.0000	2.9133	0.0000	0.0000	8.9580	0.0000	0.0000	0.014939	0.000000	0.000000
3.500	0.0432	0.0000	0.0000	2.6122	0.0000	0.0000	8.9653	0.0000	0.0000	0.013395	0.000000	0.000000
4.000	0.0431	0.0000	0.0000	2.3111	0.0000	0.0000	8.9725	0.0000	0.0000	0.011851	0.000000	0.000000
4.500	0.0424	0.0000	0.0000	2.1539	0.0000	0.0000	8.9755	0.0000	0.0000	0.011045	0.000000	0.000000
5.000	0.0418	0.0000	0.0000	1.9967	0.0000	0.0000	8.9786	0.0000	0.0000	0.010239	0.000000	0.000000

Figure 6.5 PRODAS aerodynamic lookup table based on finner model

PRODAS models the roll torque coefficient as a product of fin deflection angle with the roll coefficient derivative,

$$C_l = C_{l\delta}\delta . \tag{6.1}$$

Here C_l is the roll torque coefficient, δ is the fin cant/deflection angle, and $C_{l\delta}$ is the roll torque coefficient derivative respect to δ. The roll moment coefficients C_l due to the presence of the pins predicted by Matlab and CFD for the various freestream Mach numbers were manually input into the column named $C_{l\delta}\_F1$ in the aerodynamics lookup table. $F1$ indicates fin set number one. PRODAS allows the user to enter $C_{l\delta}$ values for up to three fin sets. Since only one fin set is present in this analysis, the values of the $C_{l\delta}\_F2$ and $C_{l\delta}\_F3$ columns were set to zero.

6.5 Opposing Pins – Yaw Performance

For yaw performance analysis, PRODAS does not allow the user to manually enter the fin normal or side force coefficients into the aerodynamic tables. Therefore a controlled trajectory, CONTRAJ, was used to simulate the yaw performance. CONTRAJ is similar to 6-DOF except it allows the user to manually specify an effective fin deflection angle at a certain time to simulate the pin force acting on the fin surface.

The net side force generated by a fin set is due to an effective fin deflection δ_{eff} and sideslip angle β. A clockwise moment generated by the side force is defined to be positive. A nose left turn is defined by a negative β and a positive y-displacement. This relation can be expressed as

$$C_Y = C_{Y\delta}\delta_{eff} - C_{Y\beta}\beta\,. \tag{6.2}$$

Here C_Y is the side force coefficient, $C_{Y\delta}$ and $C_{Y\beta}$ are the side force coefficient derivatives with respect to fin deflection angle δ and sideslip angle, β respectively. Since the projectile is symmetric and the fin chord aligns with the body axis,

$$C_{Y\delta} = C_{Y\beta} = C_{N\alpha}\,. \tag{6.3}$$

$C_{N\alpha}$ is the fin alone normal force coefficient derivative with respect to the angle of attack α. At β = 0 degrees, the second term in Equation (6.2) is reduced to zero. The simplified relation is shown in Equation (6.4)

$$C_Y = C_{Y\delta}\delta_{eff}\,. \tag{6.4}$$

The pin force can be represented by an effective fin deflection. Values of δ_{eff} can be obtained by combining Equations (6.3) and (6.4).

$$\delta_{eff} = \frac{C_Y}{C_{Y\delta}} = \frac{C_N}{C_{N\alpha}}\,. \tag{6.5}$$

C_N is the fin normal force coefficient induced by the pin shock predicted by Matlab or CFD. $C_{N\alpha}$ is calculated for the fin by PRODAS at $\alpha = 0$.

The resultant normal/side force coefficient in Equation (6.2) can be expressed as

$$C_N = C_{N\alpha}\delta_{eff} - C_{N\alpha}\beta\,. \tag{6.6}$$

The first term on the right hand side of Equation (6.6) is the force produced by the pins which CONTRAJ models as an equivalent fin deflection angle δ. Pins placed to the left of fins produce a side force to the right which translates to a counterclockwise moment (negative) on the projectile and a negative δ_{eff} value. The second term accounts for the restoring force produced by the two vertical fins, which can be considered as flat plates operating at the sideslip angle β.

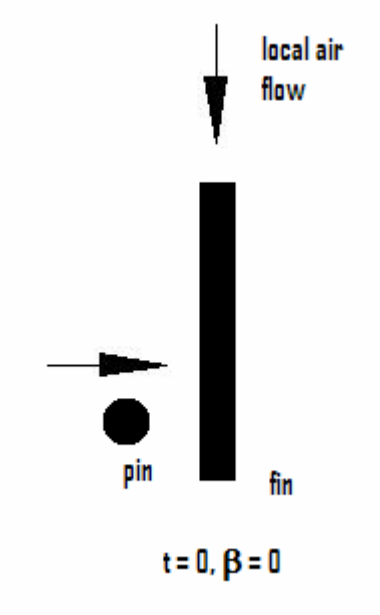

Figure 6.6 Pin force at $\beta = 0$

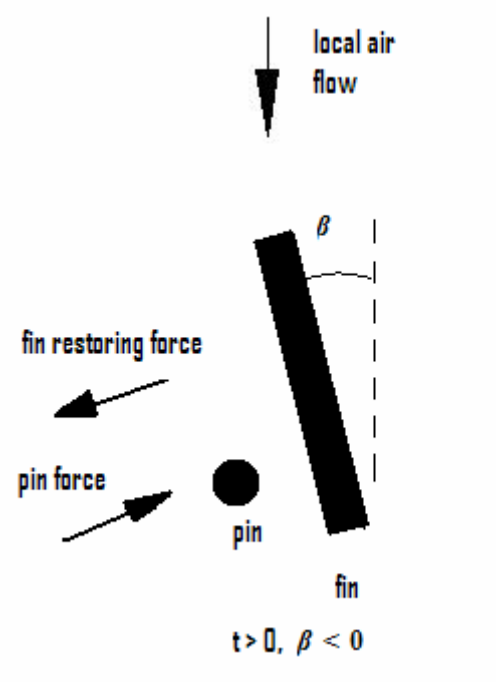

Figure 6.7 Pin and fin restoring force at $\beta < 0$

Figures 6.6 and 6.7 are illustrations of the pin and fin forces at $\beta = 0$ and $\beta < 0$. Initially at t = 0.00 s, no restoring force is produced by the vertical fins due to a zero sideslip angle. Only the pin force is present and it induces a yawing moment that pushes the projectile nose left (negative β). However, as soon as β becomes non-zero, the additional fin restoring force alters the magnitude of the side force. The fin force due to β produces a yawing moment in the opposite direction of the pin induced moment. At some value of β, the fin force would become larger than the pin force and the sideslip angle decreases to a value where the pin force again exceeds the fin force. This creates an oscillatory yawing motion.

According to Equation (6.6), a change in the net side force would produce a different control angle δ_{eff}. This variation in δ_{eff} could be approximated by using small

time steps and correcting δ_{eff} for each step. However, because of the preliminary nature of this study and the short flight time (< 1 sec), a constant δ_{eff} was assumed for the entire trajectory.

Each PRODAS simulation was for a different muzzle Mach number. Using the values for C_N from Matlab, $C_{N\alpha}$ from PRODAS and Equation (6.5), δ_{eff} values were obtained for various freestream Mach numbers. Tables 6.1 and 6.2 are the δ values for the long and short pin configurations calculated based on a zero sideslip angle.

Table 6.1 Effective fin deflection angle (long pin, *r* = 0.794 mm, 16 deg pin rotation)

Mach	C_N (Matlab)	$C_{N\alpha}$	δ_{eff} (deg)
1.5	0.0778	0.9307	-4.79
2.0	0.0570	0.8902	-3.67
2.5	0.0491	0.6310	-4.46
3.0	0.0487	0.4985	-5.60
3.5	0.0480	0.4277	-6.43
4.0	0.0467	0.3569	-7.50

Table 6.2 Effective fin deflection angle (short pin, *r* = 0.794 mm, 16 deg pin rotation)

Mach	C_N (Matlab)	$C_{N\alpha}$	δ_{eff} (deg)
1.5	0.0545	0.9307	-3.36
2.0	0.0400	0.8902	-2.58
2.5	0.0344	0.6310	-3.13
3.0	0.0341	0.4985	-3.92
3.5	0.0336	0.4277	-4.50
4.0	0.0327	0.3569	-5.25

It was expected that the calculated effective fin deflection angle would be greater for the long pin configuration than for the short pin because the fin normal force is larger. It is important to note that the projectile is also decelerating throughout the flight. As a result $C_{N\alpha}$, will not stay constant. However, the discrepancy between the muzzle and

downrange Mach number is consistently under 5 percent. Therefore it is reasonable to assume that $C_{N\alpha}$ remains constant during flight.

Figure 6.8 is a screenshot from the CONTRAJ simulations. At t = 0 sec, the control angle was set to 6.89 deg, initially inducing a nose right moment on the projectile. At t = 0.08 sec, the projectile reaches 100 m downrange. Again δ_{eff} is kept constant through the duration of the trajectory.

	Time_1	CtrlAng_1	Time_2	CtrlAng_2
Units	sec	deg	sec	deg
Red=Lock	User	User		
	0.00000	5.250	0.00000	0.000
	0.07500	5.250	0.00000	0.000
*				

Figure 6.8 CONTRAJ control angle input screenshot for M = 4.0 (short pin configuration)

6.6 Roll Trajectory Simulation Results

The 6-DOF simulations were completed for both the long and short pin configurations as the Mach number varied from 1.5 to 4.0. Fully tabulated roll performance tables are listed in Appendix E. The projectile roll angle φ (deg) at a certain downrange distance is determined by taking the integral of the spatial roll rate (deg/m) from X = 0 m to the desired downrange distance. The number of revolutions the projectile makes can be determined by dividing the total φ over the trajectory by 360 deg. Figure 6.9 shows that the long pin configuration is expected to rotate 3300 to 5000 deg over the trajectory (100 m) depending on the muzzle Mach number. This represents 9 revolutions at M = 4.0 and 14 revolutions at M = 1.5. More turns are predicted for the lower Mach numbers because the time it takes the projectile to travel downrange is

greater. Figure 6.10 shows that for the short pin model, the projectile rotates 2200 to 3400 degrees. This represents approximately 6 to 10 revolutions. This is about a 30 to 40 percent decrease from the long pin configuration due to a decrease in roll torque.

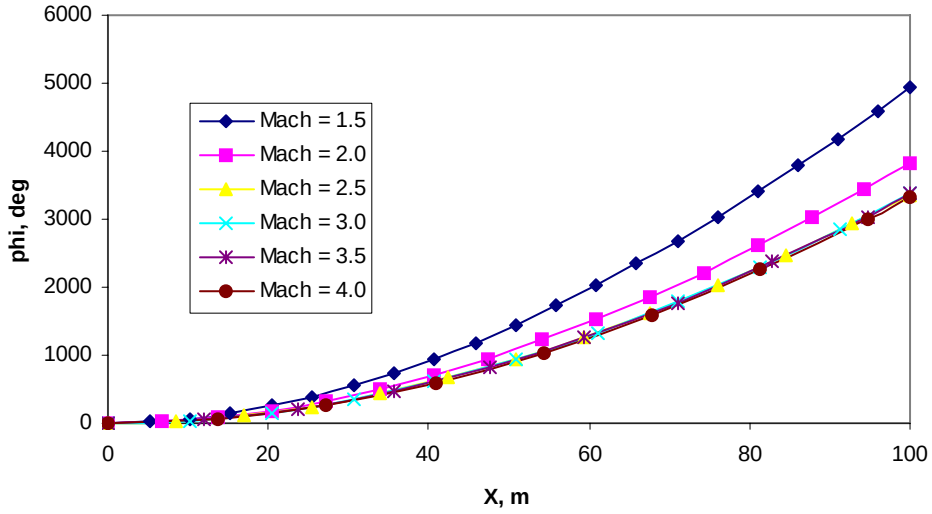

Figure 6.9 PRODAS/Matlab predicted roll angle φ vs. downrange distance X for long pin configuration (r = 0.794 mm, 16 deg pin rotation)

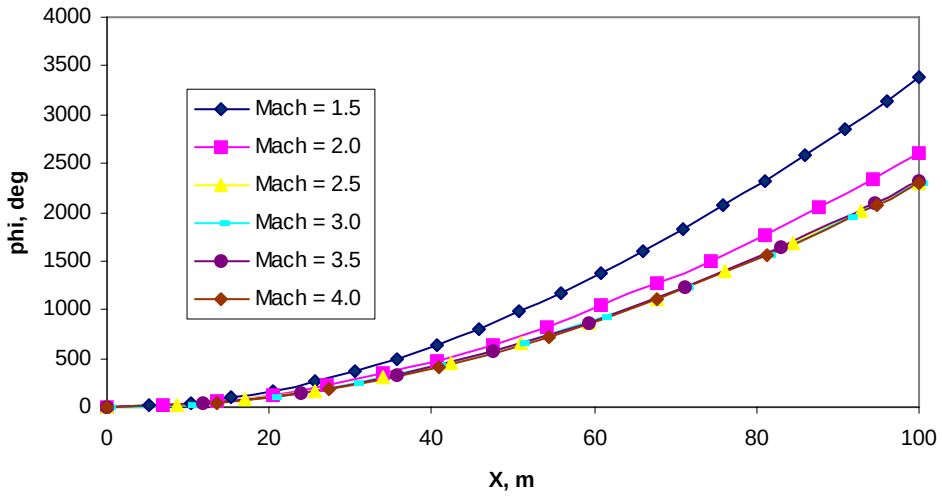

Figure 6.10 PRODAS/Matlab predicted roll angle φ vs. downrange distance X for short pin configuration (r = 0.794 mm, 16 deg pin rotation)

It is important to note that for the diametrically opposed pin configuration shown in Figures 1.1 and 1.2, a constant torque is assume to be imposed on the two fin surfaces at a given Mach number. Angular acceleration can be determined from the roll moment and moment of inertia about the longitudinal x-axis of the projectile. The angular acceleration decreases as the projectile moves downrange due to drag and other damping forces. At a certain distance downrange, the projectile reaches a steady state roll rate.

6-DOF predicted roll angles φ (using C_l from Matlab) are compared to the range test data [1] at M = 2.0, 2.4, and 2.9 for the short pin configuration. The results are shown in Table 6.3. PRODAS/Matlab underpredicted φ slightly at M = 2.0 while significantly underpredicting at M = 2.4 and 2.9. The range tests show an increase in roll angle with Mach number, while the PRODAS/Matlab simulation predicted a decrease. Silton [1] reported a similar discrepancy between the range test data and simulations. A detailed explanation was not provided. Despite the simplicity of the Matlab model, it was able to reasonably predict the magnitude of the roll angle, especially for preliminary projectile studies.

Table 6.3 PRODAS/Matlab vs. flight test roll angle φ at 100 m downrange (short pin)

Mach	Matlab φ (deg)	Silton φ (deg)	% Error
2.0	2600	2700	-3.70
2.4	2360	2800	-15.71
2.9	2305	3300	-30.15

6.7 Yaw Trajectory Simulation Results

Based on the reasonable comparisons between the Matlab predicted pin induced roll and range test data, the Matlab model was used to investigate pin induced yaw for the opposing pin configuration. The CONTRAJ trajectory simulation was performed for both the long and short pin configurations at the various muzzle Mach numbers using the C_N values predicted by the CFD and Matlab models. The fully tabulated CONTRAJ results are shown in Appendix F. It was expected that the yaw displacement would increase with Mach number due to an increase in the strength of the bow shock coming off the pins. Figure 6.11 shows that for the long pin configuration at Mach 4.0, the projectile is displaced almost 3 meters to the left at 100 meters downrange. At M = 1.5, the projectile would displace 1.2 meters as it completes its travel downrange.

The yaw displacement is predicted to be smaller for the short pin than the long pin configuration because the fin normal force is significantly smaller. Figure 6.12 shows a displacement of 2.3 m for M = 4.0 and 0.7 m for M = 1.5 at a downrange distance of 100 meters.

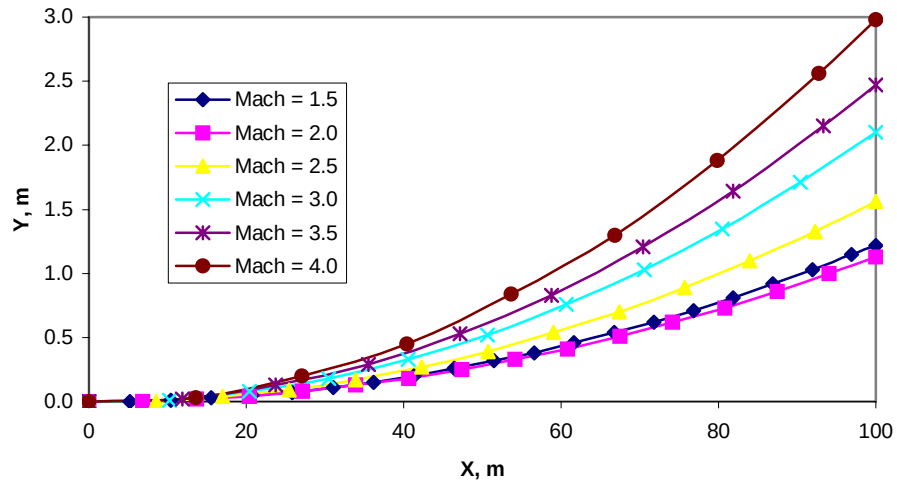

Figure 6.11 PRODAS/Matlab predicted yaw displacement *Y* vs. downrange distance *X* for long pin configuration (*r* = 0.794 mm, 16 deg pin rotation)

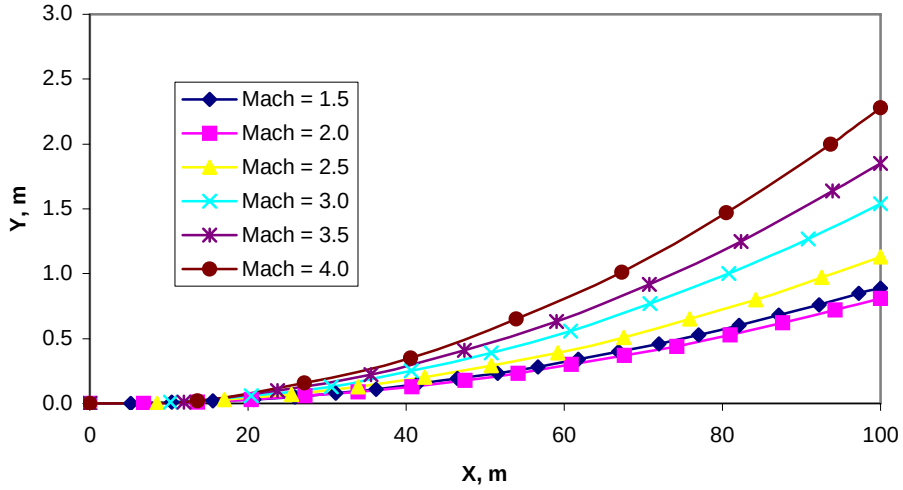

Figure 6.12 PRODAS/Matlab predicted yaw displacement *Y* vs. downrange distance *X* for short pin configuration (*r* = 0.794 mm, 16 deg pin rotation)

Plots of the sideslip angle β as a function of downrange distance for the long and short pin configurations are shown in Figures 6.13 and 6.14. The yaw oscillation is due to the opposition between the pin induced side force and fin side force illustrated in

Figures 6.6 and 6.7. It was expected that the magnitude of oscillation would increase for larger Mach numbers due to an increase in the fin normal force. Figure 6.13 shows that the maximum sideslip angle for M = 4.0 is approximately 29 degrees. This occurs at a downrange distance of approximately 14 meters. The maximum β for M = 1.5 is around only -10 degrees. Figures 6.13 and 6.14 show the sideslip angle decaying while oscillating with time. This is attributed to damping forces such as drag.

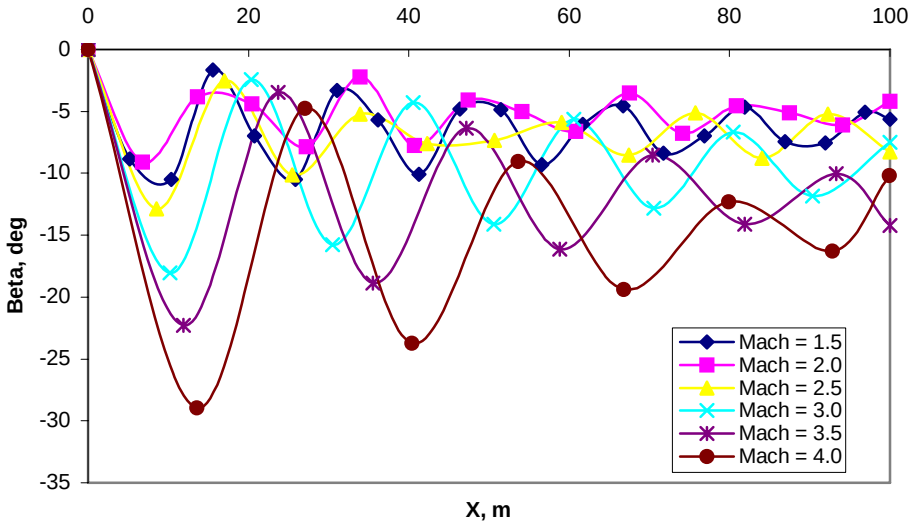

Figure 6.13 PRODAS/Matlab predicted sideslip angle β vs. downrange distance X for long pin configuration (r = 0.794 mm, 16 deg pin rotation)

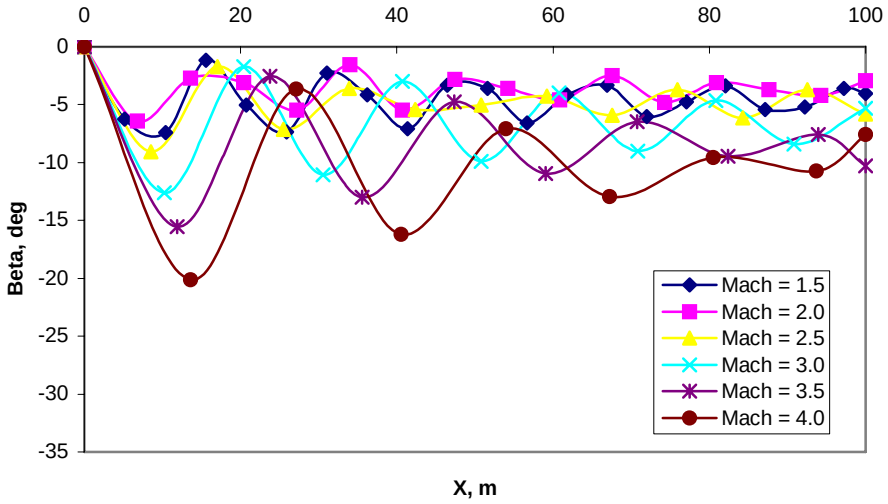

Figure 6.14 PRODAS/Matlab predicted sideslip angle β vs. downrange distance X for short pin configuration (r = 0.794 mm, 16 deg pin rotation)

The magnitude of oscillation is significantly smaller for the short pin configuration because the fin normal force is much less. This is confirmed by Figure 3.2 which shows that the long pin generates approximately 30 percent more fin normal force than the short pin configuration. Figure 6.14 shows that for the short pin configuration at M = 4.0, the maximum β is around 20 degrees (@ X = 14 m), approximately a 45 percent decrease compared to the long pin configuration.

CHAPTER VII

SUMMARY AND CONCLUSION

The major objective of this project was accomplished by showing that an opposing pin configuration was indeed able to create a normal/side force on the projectile fin surfaces. This was done by expanding upon the ARL roll torque results generated by diametrically opposed pins. A simple engineering level Matlab code was written to predict the normal force and roll torque generated by the two pin configurations. Despite the numerous assumptions, Matlab model data agreed fairly well with the benchmarked results from CFD and spark range tests. Normal force and roll torque coefficients from the Matlab model were input into a PRODAS trajectory simulation to analyze the roll and yaw performances of the projectile as it travels down a 100 m aeroballistic range.

The effects of pin height, radius, and placement on the projectile performance were analyzed as well. An increase in pin height and radius generated a higher roll torque and fin normal force as expected. However, an increase in the distance between the pin and the fin surface leads to a decrease in roll torque and fin normal force.

The idea of using control pins to replace actuators and control surfaces is still a work in progress. Future spark range tests should be performed to validate the Matlab, CFD, and PRODAS simulation results for the opposing pin configuration. Unlike this project in which the pin height was fixed, it will be much more practical if it is allowed to

vary during flight. This inherently complicates the problem because the force acting on the fin surface would fluctuate depending on the pin height.

Finally, another extension of this project would be investigating whether an opposing pin configuration for the horizontal fin set would induce a similar change in angle of attack. Pins placed above the horizontal fins would generate a normal force acting down on the horizontal fin surfaces which would induce a nose up pitching moment. On the contrary, pins placed below the horizontal fins would produce a nose down pitching moment.

APPENDIX A

MATLAB CODE

```
% estimate the force generated by control pins in the vicinity of missile
% fins at supersonic Mach numbers
clear all

% freestream conditions
freestream_pressure = input('enter freestream pressure (in Pa): ');
gamma = input('enter value of gamma: ');
Mach_number = 1.5:0.5:4; % freestream test Mach numbers
q = gamma/2*freestream_pressure*Mach_number.^2; % dynamic pressure

% projectile geometry
radius = 6.45; % body radius (mm)
noseangle = input('enter the projectile half nose angle (increments 2.5 degs up to 30): ');

% fin geometry
fin_length = input('enter the length of the fin (in mm): ');

% pin geometry
r = input('enter the radius of the pin (in mm): ');
pin_placement = input('enter degree of rotation pin is to be placed next to the fin (deg): ');
'To ensure a shock-fin interaction would occur physically, try to keep the base_distance < 3/4th
the overall length of the fin'
base_distance = input('enter distance between the center of the pin and the the base of the
projectile (mm): ');
if base_distance > (0.75*fin_length)
   ('pin placement exceeds 3/4th fin length')
   base_distance = input('enter distance between the center of the pin and the base of the
projectile (mm): ');
end

% determine the pressure and Mach number after the initial conical shock at the nose
Mach_table = [1.5, 1.5, 1.49, 1.47, 1.44, 1.4, 1.35, 1.30, 1.23, 1.16, 0, 0;
2, 2, 1.98, 1.95, 1.90, 1.84, 1.77, 1.7, 1.625, 1.53, 1.45, 1.36;
2.5, 2.49, 2.46, 2.4, 2.33, 2.24, 2.15, 2.05, 1.96, 1.86, 1.76, 1.65;
3, 2.98, 2.93, 2.84, 2.74, 2.62, 2.51, 2.39, 2.27, 2.15, 2.02, 1.9;
3.5, 3.47, 3.38, 3.26, 3.125, 2.98, 2.84, 2.69, 2.55, 2.4, 2.26, 2.12;
4, 3.94, 3.82, 3.67, 3.5, 3.32, 3.15, 2.97, 2.8, 2.63, 2.46, 2.3]; % Mach after conical shock

P_table = [1, 1, 1.01, 1.04, 1.08, 1.15, 1.23, 1.33, 1.45, 1.58, 0, 0;
1, 1.01, 1.03, 1.09, 1.17, 1.29, 1.425, 1.59, 1.77, 1.97, 2.18, 2.42;
1, 1.015, 1.065, 1.16, 1.31, 1.49, 1.7, 1.95, 2.22, 2.52, 2.84, 3.18;
1, 1.03, 1.12, 1.27, 1.48, 1.745, 2.05, 2.4, 2.78, 3.2, 3.65, 4.13;
1, 1.05, 1.18, 1.4, 1.7, 2.05, 2.46, 2.93, 3.45, 4.01, 4.62, 5.27;
1.005, 1.08, 1.27, 1.56, 1.94, 2.405, 2.94, 3.55, 4.22, 4.95, 5.74, 6.57]; % Pressure ratio after
conical shock

thetacone = 2.5:2.5:30;
index = find(thetacone == noseangle);
Mnew = transpose(Mach_table(:,index))
P1 = transpose(freestream_pressure*(P_table(:,index)))

% determine the shape of the shockwave as it moves pass the pin
num = -10:0.05:10; %mm
i = 0;
```

```
for M1 = Mnew
    i = i+1;
    Rc(i) = r*1.386*exp(1.8/((M1-1)^0.75));
    delta(i) = r*0.386*exp(4.67/M1^2);
    u(i) = asin(1/M1);
    j = 0;
    for x= -10:0.05:10
        j = j+1;
        y(i,j) = (([(r+delta(i)-x)/(Rc(i)*cot(u(i))^2)+1]^2-1) * Rc(i)^2/tan(u(i))^2)^0.5;
    end
    figure(3);
    plot(num,y(i,:),'Color',plotlinecolor(i));
    hold on;
 end

% plot flow past cylinder at various mach numbers
yfin = (2*3.14*radius)*(pin_placement/360)+r;

figure(3);
axis square;
plot(num,yfin,'k*--');
hold on;
circle([0,0],r,1000,'--');
xlabel('x distance');
ylabel('y distance');
axis([-5 5 -2 8]);

% estimating the oblique shock angles for the different Mach numbers
for i = 1:length(Mnew)
    %imag - imaginary part of array
    %find - returns all indices of array that are not zero
    %min  - finds minimum value
    maxk = min(find(imag(y(i,:))))-1;
    maxk = min(find(y(i,1:maxk)<yfin));
    slope(i) = (y(i,maxk)-y(i,maxk-1))/(0.05);
    distance(i) = (maxk-200)/20 + base_distance;
end
Beta1 = atan(slope)/pi*180;
Beta1 = -Beta1;

% determine thetamax1 from the different mach numbers
i = 0;
for M1 = Mnew
    i = i+1;
    A = 1 + (gamma-1)*M1^2/2;
    C = 1 + (gamma+1)*M1^2/2;
    U = M1^2-1;
    R = (18*A*C*U + 27*(A^2) - (U^2)*(C^2))/(4*U^3);
    thetamax1(i) = acot(sqrt((R/2)+(R^2/4+A*(C^3)/(U^3))^0.5));
    theta(i) = atan(2*cot(Beta1(i)/180*pi)*((M1^2*(sin(Beta1(i)/180*pi))^2-
1)/(M1^2*(gamma+cos(2*Beta1(i)/180*pi))+2)));
end

% calculate the values behind the initial oblique shock
M1 = Mnew;
```

```
% use oblique shock relations
% Ptemp = intermediate condition
% P2 = pressure acting on fin
% theta is a constant
Mn1 = M1.*sin(Beta1./180*pi);
Ptemp = P1.*(1+(2*gamma)/(gamma+1)*(Mn1.^2-1));
Mn2 = ((Mn1.^2+(2/(gamma-1)))/((2*gamma)/(gamma-1)*Mn1.^2-1)).^0.5;
M2 = Mn2./sin(Beta1./180*pi-theta);

% initialize pressure arrays
P2_oblique = [];
P2_case1 = [];
P2_case2 = [];

% find M2 is less than 1, then there's no reflecting shock
M2L1 = M2(find(M2<1));
PtempL1 = Ptemp(find(M2<1));
P2_oblique = PtempL1/(1000^2);

% determine if theta is greater than thetamax2
% if theta is smaller than thetamax2 then a reflecting shock would occur
% if theta is greater than thetamax2 then a normal/curve shock would occur
% - then we must use the orginal mach number to determine the pressure at
% the wall

P1g1 = P1(find(M2>1));
M2g1 = M2(find(M2>1));
thetag1 = theta(find(M2>1));
M1 = M1(find(M2>1));
Ptempg1 = Ptemp(find(M2>1));

A = 1 + (gamma-1).*M2g1.^2/2;
C = 1 + (gamma+1).*M2g1.^2/2;
U = M2g1.^2-1;
R = [18.*A.*C.*U + 27.*(A.^2) - (U.^2).*(C.^2)]./((4.*U.^3));
thetamax2 = acot(sqrt((R./2)+((R.^2/4+A.*C.^3)./(U.^3)).^0.5));

ii = 1;
jj = 0;
kk = 0;
for ii = 1:length(M2g1)

   if thetag1(ii) > thetamax2(ii)  % no oblique shock; mach reflection - case 1
      jj = jj + 1;
      M2g1_case1(jj) = M2g1(ii);
      M1_case1(jj) = M1(ii);
      P1_case1(jj) = P1g1(ii);
      P2_case1(jj) = P1_case1(jj)*(1+((2*gamma)/(gamma+1)).*(M1_case1(jj).^2-1))/(1000^2); %
N/mm^2
      M_machreflection(jj) = sqrt((1+(gamma-1)/2.*M1_case1(jj).^2)./(gamma*M1_case1(jj).^2-
(gamma-1)/2)) % final Mach number
   else                    % reflect shock - case 2
      kk = kk + 1;
      M1_case2(kk) = M1(ii);
```

```
        M2g1_case2(kk) = M2g1(ii);
        thetag1_case2(kk) = thetag1(ii);
        A(kk) = 1 + (gamma-1).*M2g1_case2(kk).^2/2;
        C(kk) = 1 + (gamma+1).*M2g1_case2(kk).^2/2;
        U(kk) = M2g1_case2(kk).^2-1;
        D(kk) = cot(thetag1_case2(kk));
        B(kk)= -D(kk).*U(kk);
        E(kk)= B(kk).^2-3.*A(kk).*C(kk);
        F(kk) = 2*(E(kk).^(3/2));
        G(kk) = 9.*A(kk).*B(kk).*C(kk) - 27.*(A(kk).^2.*D(kk)) - 2.*(B(kk).^3);
        phi(kk) = (acos(G(kk)./F(kk))+4*pi)./3;
        temp(kk) = 2.*(E(kk).^0.5).*(cos(phi(kk))-B(kk))./(3.*A(kk));
        Beta2(kk) = atan(temp(kk))./pi*180;
        M2g1_case2_n(kk) = M2g1_case2(kk).*sin(Beta2(kk).*pi/180);

        Ptempg1_case2(kk) = Ptempg1(kk);
        P2_case2(kk) = Ptempg1_case2(kk).*(1+(2*gamma)/(gamma+1).*(M2g1_case2_n(kk).^2-
1))./(1000^2); % N/mm^2
        Mn3(kk) = sqrt((1+(gamma-1)/2.*M2g1_case2_n(kk).^2)./(gamma*M2g1_case2_n(kk).^2-
(gamma-1)/2));
        M3_standardreflection(kk) = Mn3(kk)/(sin(Beta2(kk)./180*pi)-thetag1_case2(kk)) % final
Mach number
    end
ii = ii + 1;
end

if isempty(P2_oblique)
   if isempty (P2_case1)
      HH = [P2_case2];
   else
      HH = [P2_case1 P2_case2];
   end
end

if isempty(P2_case1)
    if isempty(P2_oblique)
        HH = [P2_case2];
    else
        HH = [P2_oblique P2_case2];
    end
end

if isempty(P2_case2)
    if isempty(P2_oblique)
        HH = [P2_case1];
    else
        HH = [P2_oblique P2_case1];
    end
else
    HH = [P2_oblique P2_case1 P2_case2];
end

 P1 = P1./(1e6);
HHnew = [(P1(1:2)+HH(1:2))*0.6,(P1(3:6)+HH(3:6))*0.5];
pressure_final = HHnew % final pressure acting on the fin surface
```

APPENDIX B

EXACT METHOD TO CALCULATE β FROM M AND θ

Given: M (freestream Mach number), θ (wedge half angle), and γ (ratio of specific heat)

Calculated: $\theta_{\max}$ (Maximum wedge half angle), β (shock-wave angle)

Assume: Perfect gas

Method:

$$A = 1 + \frac{(\gamma - 1)M^2}{2},$$

$$C = 1 + \frac{(\gamma + 1)M^2}{2},$$

$$U = M^2 - 1,$$

$$R = \frac{(18 \cdot A \cdot C \cdot U + 27 \cdot A^2 - U^2 \cdot C^2)}{(4 \cdot U^3)},$$

$$Cot^2\theta_{\max} = \frac{R}{2} + \left(\frac{R^2}{4} + \frac{A \cdot C^3}{U^3} \right)^{\frac{1}{2}},$$

$$D = Cot\theta,$$

$$B = -D \cdot U,$$

$$E = B^2 - 3 \cdot A \cdot C,$$

$$F = 2 \cdot E^{\frac{3}{2}},$$

$$G = 9 \cdot A \cdot B \cdot C - 27 \cdot A^2 \cdot D - 2 \cdot B^2,$$

$$\theta = \frac{\left[(\cos^{-1}(\frac{G}{F}) + 4\pi \right]}{3},$$

$$Tan\beta = \frac{\left[2 \cdot E^{\frac{1}{2}} \cos\theta - \beta \right]}{\left[3 \cdot A \right]},$$

Θ, β are in radians

APPENDIX C

MATLAB SIMULATION RESULTS

C.1 Varying Pin Length

Table C.1 Roll torque coefficient (long pin, *r* = 0.794 mm, 16 deg pin rotation)

	Mach 1.5	Mach 2	Mach 2.5	Mach 3	Mach 3.5	Mach 4
Dist Along Fin Affected by shock (mm)	6.0400	4.1900	3.5900	3.1900	2.9400	2.7900
Area of Affected by shock (mm^2)	15.3416	10.6426	9.1186	8.1026	7.4676	7.0866
Pressure on fin (N/mm^2)	0.2073	0.3025	0.4209	0.6126	0.8478	1.1036
atmospheric pressure (N/mm^2)	0.1019	0.1046	0.1098	0.1132	0.1210	0.1308
Pressure Difference (N/mm^2)	0.1054	0.1979	0.3111	0.4994	0.7268	0.9728
Force on Fin (N)	1.6169	2.1063	2.8368	4.0465	5.4276	6.8938
Roll Torque (N-m)	0.0125	0.0163	0.0219	0.0312	0.0419	0.0532
Dynamic Pressure (Pa)	159075	282800	441875	636300	866075	1131200
Roll Coefficient	**0.0466**	**0.0341**	**0.0294**	**0.0291**	**0.0287**	**0.0279**

Table C.2 Roll torque coefficient (short pin, *r* = 0.794 mm, 16 deg pin rotation)

	Mach 1.5	Mach 2	Mach 2.5	Mach 3	Mach 3.5	Mach 4
Dist Along Fin Affected by shock (mm)	6.0400	4.1900	3.5900	3.1900	2.9400	2.7900
Area of Affected by shock (mm^2)	10.7512	7.4582	6.3902	5.6782	5.2332	4.9662
Pressure on Fin (N/mm^2)	0.2073	0.3025	0.4209	0.6126	0.8478	1.1036
atmospheric pressure (N/mm^2)	0.1010	0.1010	0.1010	0.1010	0.1010	0.1010
Pressure Difference (N/mm^2)	0.1063	0.2015	0.3199	0.5116	0.7468	1.0026
Force on Fin (N)	1.1424	1.5028	2.0444	2.9052	3.9083	4.9791
Roll Torque (N-m)	0.0084	0.0110	0.0150	0.0213	0.0287	0.0365
Dynamic Pressure (Pa)	159075	282800	441875	636300	866075	1131200
Roll Coefficient	**0.0313**	**0.0231**	**0.0202**	**0.0199**	**0.0197**	**0.0192**

Table C.3 Normal force coefficient (long pin, *r* = 0.794 mm, 16 deg pin rotation)

	Mach 1.5	Mach 2	Mach 2.5	Mach 3	Mach 3.5	Mach 4
Dist Along Fin Affected by shock (mm)	6.0400	4.1900	3.5900	3.1900	2.9400	2.7900
Area affected by shock (mm^2)	15.3416	10.6426	9.1186	8.1026	7.4676	7.0866
Pressure on fin (N/mm^2)	0.2073	0.3025	0.4209	0.6126	0.8478	1.1036
atmospheric pressure (N/mm^2)	0.1019	0.1046	0.1098	0.1132	0.1210	0.1308
Pressure Difference (N/mm^2)	0.1054	0.1979	0.3111	0.4994	0.7268	0.9728
Normal force on Fin (N)	1.6169	2.1063	2.8368	4.0465	5.4276	6.8938
Dynamics Pressure (Pa)	159075	282800	441875	636300	866075	1131200
Normal Force Coefficient	**0.0778**	**0.0570**	**0.0491**	**0.0487**	**0.0480**	**0.0467**

Table C.4 Normal force coefficient (short pin, *r* = 0.794 mm, 16 deg pin rotation)

	Mach 1.5	Mach 2	Mach 2.5	Mach 3	Mach 3.5	Mach 4
Dist Along Fin Affected by shock (mm)	6.0400	4.1900	3.5900	3.1900	2.9400	2.7900
Area affected by shock (mm^2)	10.7512	7.4582	6.3902	5.6782	5.2332	4.9662
Pressure on fin (N/mm^2)	0.2073	0.3025	0.4209	0.6126	0.8478	1.1036
atmospheric pressure (N/mm^2)	0.1019	0.1046	0.1098	0.1132	0.1210	0.1308
Pressure Difference (N/mm^2)	0.1054	0.1979	0.3111	0.4994	0.7268	0.9728
Normal force on Fin (N)	1.1331	1.4761	1.9880	2.8358	3.8036	4.8311
Dynamics Pressure (Pa)	159075	282800	441875	636300	866075	1131200
Normal Force Coefficient	**0.0545**	**0.0400**	**0.0344**	**0.0341**	**0.0336**	**0.0327**

C.2 Varying Pin Radius

Table C.5 Roll torque coefficient (long pin, *r* = 1.094 mm, 16 deg pin rotation)

	Mach 1.5	Mach 2	Mach 2.5	Mach 3	Mach 3.5	Mach 4
Dist Along Fin Affected by shock (mm)	7.2900	4.9400	4.1900	3.7900	3.5400	3.3900
Area of Affected by shock (mm^2)	18.5166	12.5476	10.6426	9.6266	8.9916	8.6106
Pressure on fin (N/mm^2)	0.2077	0.3138	0.3519	0.6126	0.8478	1.1036
atmospheric pressure (N/mm^2)	0.1019	0.1046	0.1098	0.1132	0.1210	0.1308
Pressure Difference (N/mm^2)	0.1059	0.2092	0.2421	0.4994	0.7268	0.9728
Force on Fin (N)	1.9601	2.6253	2.5768	4.8076	6.5353	8.3764
Roll Torque (N-m)	0.0151	0.0203	0.0199	0.0371	0.0505	0.0647
Dynamic Pressure (Pa)	159075	282800	441875	636300	866075	1131200
Roll Coefficient	**0.0564**	**0.0425**	**0.0267**	**0.0346**	**0.0346**	**0.0339**

Table C.6 Roll torque coefficient (long pin, *r* = 0.794 mm, 16 deg pin rotation)

	Mach 1.5	Mach 2	Mach 2.5	Mach 3	Mach 3.5	Mach 4
Dist Along Fin Affected by shock (mm)	6.0400	4.1900	3.5900	3.1900	2.9400	2.7900
Area of Affected by shock (mm^2)	15.3416	10.6426	9.1186	8.1026	7.4676	7.0866
Pressure on fin (N/mm^2)	0.2073	0.3025	0.4209	0.6126	0.8478	1.1036
atmospheric pressure (N/mm^2)	0.1019	0.1046	0.1098	0.1132	0.1210	0.1308
Pressure Difference (N/mm^2)	0.1054	0.1979	0.3111	0.4994	0.7268	0.9728
Force on Fin (N)	1.6169	2.1063	2.8368	4.0465	5.4276	6.8938
Roll Torque (N-m)	0.0125	0.0163	0.0219	0.0312	0.0419	0.0532
Dynamic Pressure (Pa)	159075	282800	441875	636300	866075	1131200
Roll Coefficient	**0.0466**	**0.0341**	**0.0294**	**0.0291**	**0.0287**	**0.0279**

Table C.7 Normal force coefficient (long pin, *r* = 1.094 mm, 16 deg pin rotation)

	Mach 1.5	Mach 2	Mach 2.5	Mach 3	Mach 3.5	Mach 4
Dist Along Fin Affected by shock (mm)	7.2900	4.9400	4.1900	3.7900	3.5400	3.3900
Area affected by shock (mm^2)	18.5166	12.5476	10.6426	9.6266	8.9916	8.6106
Pressure on fin (N/mm^2)	0.2077	0.3138	0.3519	0.6126	0.8478	1.1036
atmospheric pressure (N/mm^2)	0.1019	0.1046	0.1098	0.1132	0.1210	0.1308
Pressure Difference (N/mm^2)	0.1059	0.2092	0.2421	0.4994	0.7268	0.9728
Normal force on Fin (N)	1.9601	2.6253	2.5768	4.8076	6.5353	8.3764
Dynamics Pressure (Pa)	159075	282800	441875	636300	866075	1131200
Normal Force Coefficient	**0.0943**	**0.0711**	**0.0446**	**0.0578**	**0.0578**	**0.0567**

Table C.8 Normal force coefficient (long pin, *r* = 0.794 mm, 16 deg pin rotation)

	Mach 1.5	Mach 2	Mach 2.5	Mach 3	Mach 3.5	Mach 4
Dist Along Fin Affected by shock (mm)	6.0400	4.1900	3.5900	3.1900	2.9400	2.7900
Area affected by shock (mm^2)	15.3416	10.6426	9.1186	8.1026	7.4676	7.0866
Pressure on fin (N/mm^2)	0.2073	0.3025	0.4209	0.6126	0.8478	1.1036
atmospheric pressure (N/mm^2)	0.1019	0.1046	0.1098	0.1132	0.1210	0.1308
Pressure Difference (N/mm^2)	0.1054	0.1979	0.3111	0.4994	0.7268	0.9728
Normal force on Fin (N)	1.6169	2.1063	2.8368	4.0465	5.4276	6.8938
Dynamics Pressure (Pa)	159075	282800	441875	636300	866075	1131200
Normal Force Coefficient	**0.0778**	**0.0570**	**0.0491**	**0.0487**	**0.0480**	**0.0467**

C.3 Pin Rotation Respect to Fin

Table C.9 Roll torque coefficient (long pin, *r* = 0.794 mm, 16 deg pin rotation)

	Mach 1.5	Mach 2	Mach 2.5	Mach 3	Mach 3.5	Mach 4
Dist Along Fin Affected by shock (mm)	6.0400	4.1900	3.5900	3.1900	2.9400	2.7900
Area of Affected by shock (mm^2)	15.3416	10.6426	9.1186	8.1026	7.4676	7.0866
Pressure on fin (N/mm^2)	0.2073	0.3025	0.4209	0.6126	0.8478	1.1036
atmospheric pressure (N/mm^2)	0.1019	0.1046	0.1098	0.1132	0.1210	0.1308
Pressure Difference (N/mm^2)	0.1054	0.1979	0.3111	0.4994	0.7268	0.9728
Force on Fin (N)	1.6169	2.1063	2.8368	4.0465	5.4276	6.8938
Roll Torque (N-m)	0.0125	0.0163	0.0219	0.0312	0.0419	0.0532
Dynamic Pressure (Pa)	159075	282800	441875	636300	866075	1131200
Roll Coefficient	**0.0466**	**0.0341**	**0.0294**	**0.0291**	**0.0287**	**0.0279**

Table C.10 Roll torque coefficient (long pin, *r* = 0.794 mm, 24 deg pin rotation)

	Mach 1.5	Mach 2	Mach 2.5	Mach 3	Mach 3.5	Mach 4
Dist Along Fin Affected by shock (mm)	5.9400	3.8400	2.9900	2.3900	2.0400	1.7900
Area of Affected by shock (mm^2)	15.0876	9.7536	7.5946	6.0706	5.1816	4.5466
Pressure on fin (N/mm^2)	0.2060	0.2838	0.4209	0.6126	0.8478	1.4428
atmospheric pressure (N/mm^2)	0.1019	0.1046	0.1098	0.1132	0.1210	0.1308
Pressure Difference (N/mm^2)	0.1041	0.1793	0.3111	0.4994	0.7268	1.3120
Force on Fin (N)	1.5710	1.7483	2.3627	3.0317	3.7661	5.9650
Roll Torque (N-m)	0.0121	0.0135	0.0182	0.0234	0.0291	0.0460
Dynamic Pressure (Pa)	159075	282800	441875	636300	866075	1131200
Roll Coefficient	**0.0452**	**0.0283**	**0.0245**	**0.0218**	**0.0199**	**0.0242**

Table C.11 Normal force coefficient (long pin, *r* = 0.794 mm, 16 deg pin rotation)

	Mach 1.5	Mach 2	Mach 2.5	Mach 3	Mach 3.5	Mach 4
Dist Along Fin Affected by shock (mm)	6.0400	4.1900	3.5900	3.1900	2.9400	2.7900
Area affected by shock (mm^2)	15.3416	10.6426	9.1186	8.1026	7.4676	7.0866
Pressure on fin (N/mm^2)	0.2073	0.3025	0.4209	0.6126	0.8478	1.1036
atmospheric pressure (N/mm^2)	0.1019	0.1046	0.1098	0.1132	0.1210	0.1308
Pressure Difference (N/mm^2)	0.1054	0.1979	0.3111	0.4994	0.7268	0.9728
Normal force on Fin (N)	1.6169	2.1063	2.8368	4.0465	5.4276	6.8938
Dynamics Pressure (Pa)	159075	282800	441875	636300	866075	1131200
Normal Force Coefficient	**0.0778**	**0.0570**	**0.0491**	**0.0487**	**0.0480**	**0.0467**

Table C.12 Normal force coefficient (long pin, *r* = 0.794 mm, 24 deg pin rotation)

	Mach 1.5	Mach 2	Mach 2.5	Mach 3	Mach 3.5	Mach 4
Dist Along Fin Affected by shock (mm)	5.9400	3.8400	2.9900	2.3900	2.0400	1.7900
Area affected by shock (mm^2)	15.0876	9.7536	7.5946	6.0706	5.1816	4.5466
Pressure on fin (N/mm^2)	0.2060	0.2838	0.4209	0.6126	0.8478	1.4428
atmospheric pressure (N/mm^2)	0.1019	0.1046	0.1098	0.1132	0.1210	0.1308
Pressure Difference (N/mm^2)	0.1041	0.1793	0.3111	0.4994	0.7268	1.3120
Normal force on Fin (N)	1.5710	1.7483	2.3627	3.0317	3.7661	5.9650
Dynamics Pressure (Pa)	159075	282800	441875	636300	866075	1131200
Normal Force Coefficient	**0.0756**	**0.0473**	**0.0409**	**0.0365**	**0.0333**	**0.0404**

APPENDIX D

3-D CFD SIMULATION RESULTS

D.1 Roll Torque Coefficient

Table D.1 Roll torque coefficient (long pin, *r* = 0.794 mm, 16 deg pin rotation)

M	Avg P on L_fin (Pa)	Avg P on U_fin (Pa)	Avg net F on fin (N)	L_{cp} (m)	Roll Torque (N*m)	Dynamic Pressure (Pa)	C_l
1.5	143894	133925	1.48	**0.01076**	0.0096	159075	**0.0596**
2.0	181065	145820	2.30	**0.00930**	0.0148	282800	**0.0449**
2.5	227520	157436	3.17	**0.00913**	0.0204	441875	**0.0388**
3.0	281697	166549	4.18	**0.00901**	0.0270	636300	**0.0352**
3.5	348852	182866	5.42	**0.00912**	0.0349	866075	**0.0339**
4.0	401236	199961	6.33	**0.00883**	0.0408	1131200	**0.0293**

Table D.2 Roll torque coefficient (short pin, *r* = 0.794 mm, 16 deg pin rotation)

M	Avg P on L_fin (Pa)	Avg P on U_fin (Pa)	Avg net F on fin (N)	L_{cp} (m)	Roll Torque (N*m)	Dynamic Pressure (Pa)	C_l
1.5	129212	127818	1.07	**0.00943**	0.0069	159075	**0.0377**
2.0	157508	141725	1.70	**0.00931**	0.0110	282800	**0.0332**
2.5	193755	155771	2.32	**0.00916**	0.0150	441875	**0.0286**
3.0	236869	166367	3.01	**0.00899**	0.0194	636300	**0.0252**
3.5	291191	183884	3.84	**0.00895**	0.0248	866075	**0.0236**
4.0	382783	210394	5.30	**0.00868**	0.0342	1131200	**0.0241**

D.2 Normal Force Coefficient

Table D.3 Normal force coefficient (long pin, *r* = 0.794 mm, 16 deg pin rotation)

M	Avg P on L_fin (Pa)	Avg P on U_fin (Pa)	Avg net F on fin (N)	Dynamic pressure (Pa)	C_n
1.5	143894	133925	1.48	159075	**0.0714**
2.0	181065	145820	2.30	282800	**0.0623**
2.5	227520	157436	3.17	441875	**0.0549**
3.0	281697	166549	4.18	636300	**0.0503**
3.5	348852	182866	5.42	866075	**0.0479**
4.0	401236	199961	6.33	1131200	**0.0428**

Table D.4 Normal force coefficient (short pin, *r* = 0.794 mm, 16 deg pin rotation)

M	Avg P on L_fin (Pa)	Avg P on U_fin (Pa)	Avg net F on fin (N)	Dynamic pressure (Pa)	C_n
1.5	129212	127818	1.07	159075	**0.0515**
2.0	157508	141725	1.70	282800	**0.0460**
2.5	193755	155771	2.32	441875	**0.0402**
3.0	236869	166367	3.01	636300	**0.0362**
3.5	291191	183884	3.84	866075	**0.0339**
4.0	382783	210394	5.30	1131200	**0.0359**

APPENDIX E

6-DOF ROLL PERFORMANCE RESULTS (MATLAB/PRODAS)

E.1 Long Pin Roll Performance

Table E.1 Roll (*M* = 1.5, long pin, *r* = 0.794 mm, 16 deg pin rotation)

Distance (m)	Spin Rate (deg/m)	Roll angle φ (deg)
0	0	0
5.12	6.40	17.66
10.23	12.59	66.71
15.33	18.55	145.91
20.42	24.24	254.05
25.51	29.68	390.24
30.59	34.88	553.09
35.66	39.85	741.44
40.73	44.59	954.55
45.79	49.12	1190.93
50.84	53.43	1449.42
55.88	57.55	1728.89
60.92	61.47	2028.82
65.95	65.20	2347.58
70.97	68.76	2684.05
75.98	72.14	3037.14
80.99	75.35	3406.52
85.99	78.40	3790.42
90.99	81.30	4188.61
95.98	84.04	4599.25
100.00	86.15	4939.05

Table E.2 Roll (*M* = 2.0, long pin, *r* = 0.794 mm, 16 deg pin rotation)

Distance (m)	Spin Rate (deg/m)	Roll angle φ (deg)
0	0	0
6.81	6.22	22.04
13.62	12.16	84.59
20.41	17.85	185.98
27.19	23.29	324.78
33.96	28.51	499.52
40.72	33.50	708.73
47.46	38.28	950.59
54.20	42.87	1224.39
60.92	47.26	1527.88
67.63	51.46	1860.04
74.34	55.49	2220.03
81.03	59.36	2605.39
87.71	63.06	3015.27
94.37	66.62	3447.64
100.00	69.50	3830.69

Table E.3 Roll (*M* = 2.5, long pin, *r* = 0.794 mm, 16 deg pin rotation)

Distance (m)	Spin Rate (deg/m)	Roll angle φ (deg)
0	0	0
8.51	6.68	29.12
17.01	13.04	112.81
25.49	19.09	248.59
33.96	24.85	434.27
42.41	30.32	667.31
50.84	35.54	945.33
59.26	40.50	1266.39
67.67	45.23	1628.29
76.05	49.72	2027.88
84.43	54.00	2464.38
92.79	58.08	2934.62
100.00	61.45	3366.54

Table E.4 Roll (*M* = 3.0, long pin, *r* = 0.794 mm, 16 deg pin rotation)

Distance (m)	Spin Rate (deg/m)	Roll angle φ (deg)
0	0	0
10.22	7.93	41.20
20.42	15.43	160.18
30.60	22.53	353.12
40.76	29.25	616.19
50.90	35.60	945.64
61.02	41.62	1337.75
71.13	47.31	1789.31
81.21	52.69	2295.79
91.27	57.78	2853.99
100.00	61.98	3378.57

Table E.5 Roll (*M* = 3.5, long pin, *r* = 0.794 mm, 16 deg pin rotation)

Distance (m)	Spin Rate (deg/m)	Roll angle φ (deg)
0	0	0
11.92	9.10	54.90
23.81	17.70	213.93
35.68	25.81	471.53
47.52	33.46	821.86
59.34	40.69	1259.65
71.13	47.50	1779.05
82.90	53.93	2375.07
94.64	60.00	3041.83
100.00	62.66	3368.92

Table E.6 Roll (*M* = 4.0, long pin, *r* = 0.794 mm, 16 deg pin rotation)

Distance (m)	Spin Rate (deg/m)	Roll angle φ (deg)
0	0	0
13.62	10.07	69.24
27.22	19.61	271.12
40.78	28.62	597.94
54.32	37.10	1042.89
67.82	45.11	1598.10
81.29	52.66	2256.74
94.74	59.77	3012.37
100.00	62.45	3333.14

E.2 Short Pin Roll Performance

Table E.7 Roll (*M* = 1.5, short pin, *r* = 0.794 mm, 16 deg pin rotation)

Distance (m)	Spin Rate (deg/m)	Roll angle φ (deg)
0	0	0
5.12	4.30	11.84
10.23	8.46	44.75
15.33	12.46	97.96
20.42	16.30	170.73
25.51	19.99	262.51
30.59	23.52	372.42
35.66	26.91	499.74
40.73	30.16	644.04
45.79	33.27	804.35
50.84	36.25	979.97
55.88	39.10	1170.17
60.92	41.84	1374.69
65.95	44.45	1592.46
70.97	46.96	1822.79
75.98	49.35	2064.99
80.99	51.65	2318.92
85.99	53.84	2583.42
90.99	55.93	2858.39
95.98	57.93	3142.65
100.00	59.48	3378.40

Table E.8 Roll (*M* = 2.0, short pin, *r* = 0.794 mm, 16 deg pin rotation)

Distance (m)	Spin Rate (deg/m)	Roll angle φ (deg)
0	0	0
6.81	4.21	14.94
13.62	8.24	57.33
20.41	12.09	126.05
27.19	15.78	220.14
33.96	19.31	338.63
40.72	22.69	480.54
47.46	25.93	644.63
54.20	29.03	830.45
60.92	32.00	1036.49
67.63	34.85	1262.06
74.34	37.58	1506.62
81.03	40.20	1768.51
87.71	42.71	2047.16
94.37	45.11	2341.21
100.00	47.07	2601.81

Table E.9 Roll (*M* = 2.5, short pin, *r* = 0.794 mm, 16 deg pin rotation)

Distance (m)	Spin Rate (deg/m)	Roll angle φ (deg)
0	0	0
8.52	4.59	20.04
17.02	8.96	77.54
25.51	13.12	170.88
33.98	17.07	298.30
42.43	20.82	458.11
50.87	24.40	648.88
59.30	27.80	869.05
67.71	31.03	1116.78
76.10	34.11	1390.43
84.48	37.04	1688.79
92.84	39.82	2009.96
100.00	42.10	2302.63

Table E.10 Roll (*M* = 3.0, short pin, *r* = 0.794 mm, 16 deg pin rotation)

Distance (m)	Spin Rate (deg/m)	Roll angle φ (deg)
0	0	0
10.22	5.42	28.17
20.42	10.55	109.50
30.60	15.41	241.35
40.76	20.00	421.12
50.90	24.35	646.21
61.02	28.46	914.07
71.13	32.35	1222.50
81.21	36.04	1568.38
91.27	39.52	1949.52
100.00	42.40	2307.64

Table E.11 Roll (*M* = 3.5, short pin, *r* = 0.794 mm, 16 deg pin rotation)

Distance (m)	Spin Rate (deg/m)	Roll angle φ (deg)
0	0	0
11.92	6.25	37.68
23.81	12.15	146.96
35.68	17.72	324.13
47.52	22.98	565.27
59.34	27.94	866.86
71.13	32.61	1224.98
82.90	37.03	1636.30
94.64	41.19	2096.87
100.00	43.00	2322.98

Table E.12 Roll (*M* = 4.0, short pin, *r* = 0.794 mm, 16 deg pin rotation)

Distance (m)	Spin Rate (deg/m)	Roll angle φ (deg)
0	0	0
13.62	6.94	47.73
27.22	13.51	186.75
40.78	19.70	411.75
54.32	25.54	718.00
67.82	31.05	1100.07
81.29	36.24	1553.24
94.74	41.13	2073.03
100.00	42.98	2293.66

APPENDIX F

CONTRAJ YAW PERFORMANCE RESULTS (MATLAB/PRODAS)

F.1 Long Pin Yaw Performance

Table F.1 Yaw (*M* = 1.5, long pin, *r* = 0.794 mm, 16 deg pin rotation)

Input		Output									
Time_1	CtrlAng_1	Time	X	Y	Z	Velocity	Spin	AlphaBar	Alpha	Beta	Mach
sec	Deg	sec	m	m	m	m/sec	deg/sec	deg	deg	deg	
0	4.76	0.00	0.00	**0.00**	0.00	0.00	520.50	0.00	0.00	**0.00**	1.53
0.2	4.76	0.01	5.20	**0.00**	0.00	5.20	519.60	8.84	0.01	**-8.84**	1.53
		0.02	10.39	**0.01**	0.00	10.39	517.99	10.51	0.00	**-10.51**	1.52
		0.03	15.56	**0.03**	0.00	15.56	516.98	1.67	0.00	**-1.67**	1.52
		0.04	20.73	**0.05**	-0.01	20.73	516.12	7.00	0.00	**-7.00**	1.52
		0.05	25.88	**0.07**	-0.01	25.88	514.72	10.51	0.00	**-10.51**	1.51
		0.06	31.02	**0.11**	-0.02	31.02	513.64	3.30	0.00	**-3.30**	1.51
		0.07	36.16	**0.15**	-0.02	36.16	512.80	5.67	0.00	**-5.67**	1.51
		0.08	41.28	**0.20**	-0.03	41.28	511.57	10.07	0.00	**-10.07**	1.50
		0.09	46.39	**0.26**	-0.04	46.39	510.44	4.80	0.00	**-4.80**	1.50
		0.10	51.49	**0.32**	-0.05	51.49	509.59	4.86	0.00	**-4.86**	1.50
		0.11	56.58	**0.38**	-0.06	56.58	508.50	9.32	0.00	**-9.32**	1.49
		0.12	61.66	**0.46**	-0.07	61.66	507.34	6.07	0.00	**-6.07**	1.49
		0.13	66.72	**0.54**	-0.08	66.73	506.46	4.54	0.00	**-4.54**	1.49
		0.14	71.78	**0.62**	-0.09	71.79	505.46	8.40	0.00	**-8.40**	1.49
		0.15	76.83	**0.71**	-0.11	76.84	504.31	7.00	0.00	**-7.00**	1.48
		0.16	81.87	**0.81**	-0.12	81.87	503.40	4.66	0.00	**-4.66**	1.48
		0.17	86.90	**0.92**	-0.14	86.90	502.46	7.47	0.00	**-7.47**	1.48
		0.18	91.92	**1.03**	-0.16	91.92	501.35	7.55	0.00	**-7.55**	1.47
		0.19	96.92	**1.15**	-0.17	96.93	500.40	5.07	0.00	**-5.07**	1.47
		0.20	99.99	**1.22**	-0.18	100.00	499.86	5.64	0.00	**-5.64**	1.47

Table F.2 Yaw (*M* = 2.0, long pin, *r* = 0.794 mm, 16 deg pin rotation)

Input		Output									
Time_1	CtrlAng_1	Time	X	Y	Z	Velocity	Spin	AlphaBar	Alpha	Beta	Mach
sec	Deg	sec	m	m	m	m/sec	deg/sec	deg	deg	deg	
0	3.67	0.00	0.00	**0.00**	0.00	0.00	682.50	0.00	0.00	**0.00**	2.01
0.15	3.67	0.01	6.82	**0.00**	0.00	6.82	681.09	9.11	0.00	**-9.11**	2.00
		0.02	13.62	**0.02**	0.00	13.62	679.23	3.85	0.00	**-3.85**	2.00
		0.03	20.41	**0.04**	0.00	20.41	678.01	4.37	0.00	**-4.37**	1.99
		0.04	27.18	**0.08**	-0.01	27.18	676.27	7.86	0.00	**-7.86**	1.99
		0.05	33.93	**0.13**	-0.01	33.93	674.90	2.22	0.00	**-2.22**	1.98
		0.06	40.67	**0.18**	-0.02	40.68	673.49	7.78	0.00	**-7.78**	1.98
		0.07	47.40	**0.25**	-0.02	47.40	671.90	4.09	0.00	**-4.09**	1.97
		0.08	54.11	**0.33**	-0.03	54.11	670.64	5.02	0.00	**-5.02**	1.97
		0.09	60.81	**0.41**	-0.04	60.81	669.06	6.64	0.00	**-6.64**	1.97
		0.10	67.49	**0.51**	-0.05	67.50	667.72	3.50	0.00	**-3.50**	1.96
		0.11	74.16	**0.62**	-0.06	74.17	666.33	6.79	0.00	**-6.79**	1.96
		0.12	80.82	**0.73**	-0.07	80.82	664.85	4.53	0.00	**-4.53**	1.95
		0.13	87.46	**0.86**	-0.08	87.46	663.57	5.13	0.00	**-5.13**	1.95
		0.14	94.09	**1.00**	-0.09	94.09	662.09	6.09	0.00	**-6.09**	1.95
		0.15	99.99	**1.13**	-0.11	100.00	660.89	4.18	0.00	**-4.18**	1.94

Table F.3 Yaw (*M* = 2.5, long pin, *r* = 0.794 mm, 16 deg pin rotation)

Input		Output									
Time_1	CtrlAng_1	Time	X	Y	Z	Velocity	Spin	AlphaBar	Alpha	Beta	Mach
sec	deg	Sec	m	m	m	m/sec	deg/sec	deg	deg	deg	
0	4.46	0.00	0.00	**0.00**	0.00	0.00	852.50	0.00	0.00	**0.00**	2.51
0.12	4.46	0.01	8.52	**0.00**	0.00	8.52	850.09	12.89	0.00	**-12.89**	2.50
		0.02	17.00	**0.04**	0.00	17.00	847.14	2.51	0.00	**-2.51**	2.49
		0.03	25.46	**0.09**	0.00	25.46	845.14	10.13	0.00	**-10.13**	2.48
		0.04	33.90	**0.17**	-0.01	33.90	842.17	5.22	0.00	**-5.22**	2.48
		0.05	42.31	**0.27**	-0.01	42.31	840.31	7.59	0.00	**-7.59**	2.47
		0.06	50.70	**0.39**	-0.02	50.70	837.48	7.35	0.00	**-7.35**	2.46
		0.07	59.06	**0.54**	-0.02	59.06	835.57	5.87	0.00	**-5.87**	2.46
		0.08	67.40	**0.70**	-0.03	67.41	832.98	8.54	0.00	**-8.54**	2.45
		0.09	75.72	**0.89**	-0.04	75.72	830.93	5.12	0.00	**-5.12**	2.44
		0.10	84.01	**1.10**	-0.05	84.02	828.58	8.79	0.00	**-8.79**	2.44
		0.11	92.28	**1.33**	-0.06	92.29	826.40	5.21	0.00	**-5.21**	2.43
		0.12	99.99	**1.56**	-0.07	100.00	824.39	8.27	0.00	**-8.27**	2.42

Table F.4 Yaw (*M* = 3.0, long pin, *r* = 0.794 mm, 16 deg pin rotation)

Input		Output									
Time_1	CtrlAng_1	Time	X	Y	Z	Velocity	Spin	AlphaBar	Alpha	Beta	Mach
sec	deg	Sec	m	m	m	m/sec	deg/sec	deg	deg	deg	
0	5.6	0.00	0.00	**0.00**	0.00	0.00	1023.00	0.00	0.00	**0.00**	3.01
0.1	5.6	0.01	10.21	**0.01**	0.00	10.21	1018.65	18.02	0.00	**-18.02**	2.99
		0.02	20.37	**0.08**	0.00	20.37	1014.01	2.45	0.00	**-2.45**	2.98
		0.03	30.50	**0.18**	0.00	30.50	1010.10	15.78	0.00	**-15.78**	2.97
		0.04	40.57	**0.33**	-0.01	40.57	1005.77	4.27	0.00	**-4.27**	2.96
		0.05	50.61	**0.52**	-0.01	50.61	1002.13	14.09	0.00	**-14.09**	2.95
		0.06	60.61	**0.76**	-0.02	60.61	998.01	5.65	0.00	**-5.65**	2.93
		0.07	70.57	**1.03**	-0.02	70.57	994.52	12.80	0.00	**-12.80**	2.92
		0.08	80.48	**1.35**	-0.03	80.50	990.54	6.68	0.00	**-6.68**	2.91
		0.09	90.37	**1.71**	-0.04	90.38	987.15	11.83	0.00	**-11.83**	2.90
		0.10	99.98	**2.10**	-0.05	100.00	983.35	7.52	0.00	**-7.52**	2.89

Table F.5 Yaw (*M* = 3.5, long pin, *r* = 0.794 mm, 16 deg pin rotation)

Input		Output									
Time_1	CtrlAng_1	Time	X	Y	Z	Velocity	Spin	AlphaBar	Alpha	Beta	Mach
sec	deg	Sec	m	m	m	m/sec	deg/sec	deg	deg	deg	
0	6.43	0.00	0.00	**0.00**	0.00	0.00	1193.50	0.00	0.00	**0.00**	3.51
0.085	6.43	0.01	11.91	**0.02**	0.00	11.91	1186.17	22.29	0.00	**-22.29**	3.49
		0.02	23.73	**0.13**	0.00	23.73	1179.47	3.45	0.00	**-3.45**	3.47
		0.03	35.49	**0.29**	0.00	35.49	1172.11	18.85	0.00	**-18.85**	3.44
		0.04	47.18	**0.53**	-0.01	47.18	1166.61	6.35	0.00	**-6.35**	3.43
		0.05	58.81	**0.83**	-0.01	58.82	1159.47	16.11	0.00	**-16.11**	3.41
		0.06	70.37	**1.21**	-0.02	70.38	1154.52	8.54	0.00	**-8.54**	3.39
		0.07	81.88	**1.64**	-0.02	81.89	1147.70	14.13	0.00	**-14.13**	3.37
		0.08	93.32	**2.15**	-0.03	93.34	1142.94	10.02	0.00	**-10.02**	3.36
		0.086	99.97	**2.47**	-0.03	100.00	1139.32	14.21	0.00	**-14.21**	3.35

Table F.6 Yaw (*M* = 4.0, long pin, *r* = 0.794 mm, 16 deg pin rotation)

Input		Output									
Time_1	CtrlAng_1	Time	X	Y	Z	Velocity	Spin	AlphaBar	Alpha	Beta	Mach
sec	deg	Sec	m	m	m	m/sec	deg/sec	deg	deg	deg	
0	7.5	0.00	0.00	**0.00**	0.00	0.00	1364.00	0.00	0.00	**0.00**	4.01
0.076	7.5	0.01	13.60	**0.03**	0.00	13.60	1352.26	28.96	0.00	**-28.96**	3.97
		0.02	27.05	**0.20**	0.00	27.05	1341.89	4.76	0.00	**-4.76**	3.94
		0.03	40.42	**0.45**	0.00	40.43	1329.76	23.75	0.00	**-23.75**	3.91
		0.04	53.66	**0.84**	-0.01	53.67	1321.50	9.05	0.00	**-9.05**	3.88
		0.05	66.82	**1.30**	-0.01	66.83	1309.33	19.41	0.00	**-19.41**	3.85
		0.06	79.86	**1.88**	-0.02	79.88	1302.06	12.31	0.00	**-12.31**	3.83
		0.07	92.80	**2.56**	-0.02	92.84	1290.50	16.30	0.00	**-16.30**	3.79
		0.076	99.96	**2.98**	-0.03	100.00	1286.45	10.20	0.00	**-10.20**	3.78

F.2 Short Pin Yaw Performance

Table F.7 Yaw (*M* = 1.5, short pin, *r* = 0.794 mm, 16 deg pin rotation)

Input		Output									
Time_1	CtrlAng_1	Time	X	Y	Z	Velocity	Spin	AlphaBar	Alpha	Beta	Mach
sec	deg	Sec	m	m	m	m/sec	deg/sec	deg	deg	deg	
0	3.36	0.00	0.00	**0.00**	0.00	0.00	520.50	0.00	0.00	**0.00**	1.53
0.2	3.36	0.01	5.20	**0.00**	0.00	5.20	519.67	6.26	0.01	**-6.26**	1.53
		0.02	10.39	**0.01**	0.00	10.39	518.49	7.39	0.00	**-7.39**	1.52
		0.03	15.57	**0.02**	0.00	15.57	517.61	1.17	0.00	**-1.17**	1.52
		0.04	20.74	**0.03**	-0.01	20.74	516.81	5.01	0.00	**-5.01**	1.52
		0.05	25.91	**0.05**	-0.01	25.91	515.73	7.37	0.00	**-7.37**	1.52
		0.06	31.06	**0.08**	-0.02	31.06	514.82	2.28	0.00	**-2.28**	1.51
		0.07	36.20	**0.11**	-0.02	36.20	514.03	4.12	0.00	**-4.12**	1.51
		0.08	41.34	**0.15**	-0.03	41.34	513.04	7.08	0.00	**-7.08**	1.51
		0.09	46.46	**0.19**	-0.04	46.46	512.11	3.29	0.00	**-3.29**	1.51
		0.10	51.58	**0.23**	-0.05	51.58	511.32	3.57	0.00	**-3.57**	1.50
		0.11	56.69	**0.28**	-0.06	56.69	510.39	6.60	0.00	**-6.60**	1.50
		0.12	61.79	**0.34**	-0.07	61.79	509.45	4.14	0.00	**-4.14**	1.50
		0.13	66.88	**0.40**	-0.08	66.88	508.65	3.33	0.00	**-3.33**	1.50
		0.14	71.96	**0.46**	-0.09	71.96	507.77	6.02	0.00	**-6.02**	1.49
		0.15	77.03	**0.53**	-0.11	77.04	506.84	4.77	0.00	**-4.77**	1.49
		0.16	82.10	**0.60**	-0.12	82.10	506.02	3.35	0.00	**-3.35**	1.49
		0.17	87.15	**0.68**	-0.14	87.16	505.18	5.42	0.00	**-5.42**	1.49
		0.18	92.20	**0.76**	-0.16	92.20	504.26	5.18	0.00	**-5.18**	1.48
		0.19	97.24	**0.85**	-0.17	97.24	503.43	3.57	0.00	**-3.57**	1.48
		0.20	100.00	**0.89**	-0.18	100.00	502.99	4.04	0.00	**-4.04**	1.48

Table F.8 Yaw (*M* = 2.0, short pin, *r* = 0.794 mm, 16 deg pin rotation)

Input		Output									
Time_1	CtrlAng_1	Time	X	Y	Z	Velocity	Spin	AlphaBar	Alpha	Beta	Mach
sec	deg	Sec	m	m	m	m/sec	deg/sec	deg	deg	deg	
0	2.58	0.00	0.00	**0.00**	0.00	0.00	682.50	0.00	0.00	**0.00**	2.01
0.15	2.58	0.01	6.82	**0.00**	0.00	6.82	681.22	6.41	0.00	**-6.41**	2.00
		0.02	13.62	**0.01**	0.00	13.62	679.73	2.69	0.00	**-2.69**	2.00
		0.03	20.41	**0.03**	0.00	20.41	678.55	3.11	0.00	**-3.11**	1.99
		0.04	27.19	**0.06**	-0.01	27.19	677.11	5.49	0.00	**-5.49**	1.99
		0.05	33.96	**0.09**	-0.01	33.96	675.87	1.57	0.00	**-1.57**	1.99
		0.06	40.71	**0.13**	-0.02	40.71	674.60	5.49	0.00	**-5.49**	1.98
		0.07	47.45	**0.18**	-0.02	47.45	673.24	2.82	0.00	**-2.82**	1.98
		0.08	54.18	**0.23**	-0.03	54.18	672.05	3.61	0.00	**-3.61**	1.98
		0.09	60.89	**0.30**	-0.04	60.89	670.70	4.61	0.00	**-4.61**	1.97
		0.10	67.59	**0.37**	-0.05	67.59	669.47	2.49	0.00	**-2.49**	1.97
		0.11	74.28	**0.44**	-0.06	74.28	668.22	4.80	0.00	**-4.80**	1.96
		0.12	80.95	**0.53**	-0.07	80.95	666.93	3.12	0.00	**-3.12**	1.96
		0.13	87.62	**0.62**	-0.08	87.62	665.73	3.70	0.00	**-3.70**	1.96
		0.14	94.27	**0.72**	-0.09	94.27	664.44	4.22	0.00	**-4.22**	1.95
		0.15	100.00	**0.81**	-0.11	100.00	663.39	2.95	0.00	**-2.95**	1.95

Table F.9 Yaw (*M* = 2.5, short pin, *r* = 0.794 mm, 16 deg pin rotation)

Input		Output									
Time_1	CtrlAng_1	Time	X	Y	Z	Velocity	Spin	AlphaBar	Alpha	Beta	Mach
sec	deg	Sec	m	m	m	m/sec	deg/sec	deg	deg	deg	
0	3.13	0.00	0.00	**0.00**	0.00	0.00	852.50	0.00	0.00	**0.00**	2.51
0.12	3.13	0.01	8.52	**0.00**	0.00	8.52	850.52	9.05	0.00	**-9.05**	2.50
		0.02	17.01	**0.03**	0.00	17.01	848.28	1.74	0.00	**-1.74**	2.49
		0.03	25.48	**0.07**	0.00	25.48	846.50	7.16	0.00	**-7.16**	2.49
		0.04	33.94	**0.13**	-0.01	33.94	844.25	3.59	0.00	**-3.59**	2.48
		0.05	42.37	**0.20**	-0.01	42.37	842.54	5.44	0.00	**-5.44**	2.48
		0.06	50.78	**0.29**	-0.02	50.78	840.37	5.05	0.00	**-5.05**	2.47
		0.07	59.18	**0.39**	-0.02	59.18	838.64	4.25	0.00	**-4.25**	2.46
		0.08	67.55	**0.51**	-0.03	67.56	836.58	5.90	0.00	**-5.90**	2.46
		0.09	75.91	**0.65**	-0.04	75.91	834.80	3.70	0.00	**-3.70**	2.45
		0.10	84.25	**0.80**	-0.05	84.25	832.85	6.12	0.00	**-6.12**	2.45
		0.11	92.56	**0.97**	-0.06	92.57	831.01	3.70	0.00	**-3.70**	2.44
		0.12	99.99	**1.13**	-0.07	100.00	829.37	5.82	0.00	**-5.82**	2.44

Table F.10 Yaw (*M* = 3.0, short pin, *r* = 0.794 mm, 16 deg pin rotation)

Input		Output									
Time_1	CtrlAng_1	Time	X	Y	Z	Velocity	Spin	AlphaBar	Alpha	Beta	Mach
sec	deg	Sec	m	m	m	m/sec	deg/sec	deg	deg	deg	
0	3.92	0.00	0.00	**0.00**	0.00	0.00	1023.00	0.00	0.00	**0.00**	3.01
0.1	3.92	0.01	10.22	**0.01**	0.00	10.22	1019.83	12.60	0.00	**-12.60**	3.00
		0.02	20.40	**0.06**	0.00	20.40	1016.54	1.73	0.00	**-1.73**	2.99
		0.03	30.55	**0.13**	0.00	30.55	1013.57	11.05	0.00	**-11.05**	2.98
		0.04	40.67	**0.25**	-0.01	40.67	1010.46	3.01	0.00	**-3.01**	2.97
		0.05	50.76	**0.39**	-0.01	50.76	1007.62	9.90	0.00	**-9.90**	2.96
		0.06	60.81	**0.56**	-0.02	60.82	1004.61	3.96	0.00	**-3.96**	2.95
		0.07	70.85	**0.77**	-0.02	70.85	1001.85	9.03	0.00	**-9.03**	2.94
		0.08	80.85	**1.00**	-0.03	80.85	998.92	4.66	0.00	**-4.66**	2.94
		0.09	90.82	**1.27**	-0.04	90.83	996.20	8.38	0.00	**-8.38**	2.93
		0.10	99.99	**1.54**	-0.05	100.00	993.52	5.32	0.00	**-5.32**	2.92

Table F.11 Yaw (*M* = 3.5, short pin, *r* = 0.794 mm, 16 deg pin rotation)

Input		Output									
Time_1	CtrlAng_1	Time	X	Y	Z	Velocity	Spin	AlphaBar	Alpha	Beta	Mach
sec	deg	Sec	m	m	m	m/sec	deg/sec	deg	deg	deg	
0	4.5	0.00	0.00	**0.00**	0.00	0.00	1193.00	0.00	0.00	**0.00**	3.51
0.085	4.5	0.01	11.91	**0.01**	0.00	11.91	1187.98	15.53	0.00	**-15.53**	3.49
		0.02	23.76	**0.10**	0.00	23.76	1183.38	2.55	0.00	**-2.55**	3.48
		0.03	35.57	**0.22**	0.00	35.58	1178.36	13.00	0.00	**-13.00**	3.46
		0.04	47.33	**0.41**	-0.01	47.34	1174.43	4.76	0.00	**-4.76**	3.45
		0.05	59.05	**0.63**	-0.01	59.06	1169.51	10.94	0.00	**-10.94**	3.44
		0.06	70.73	**0.92**	-0.02	70.73	1165.85	6.45	0.00	**-6.45**	3.43
		0.07	82.36	**1.25**	-0.02	82.37	1161.11	9.48	0.00	**-9.48**	3.41
		0.08	93.94	**1.64**	-0.03	93.96	1157.51	7.56	0.00	**-7.56**	3.40
		0.085	99.98	**1.85**	-0.03	100.00	1155.18	10.27	0.00	**-10.27**	3.40

Table F.12 Yaw (*M* = 4.0, short pin, *r* = 0.794 mm, 16 deg pin rotation)

Input		Output									
Time_1	CtrlAng_1	Time	X	Y	Z	Velocity	Spin	AlphaBar	Alpha	Beta	Mach
sec	deg	sec	m	m	m	m/sec	deg/sec	deg	deg	deg	
0	5.25	0.00	0.00	**0.00**	0.00	0.00	1364.00	0.00	0.00	**0.00**	4.01
0.075	5.25	0.01	13.61	**0.02**	0.00	13.61	1355.81	20.10	0.00	**-20.10**	3.98
		0.02	27.12	**0.16**	0.00	27.12	1348.77	3.65	0.00	**-3.65**	3.96
		0.03	40.58	**0.35**	0.00	40.58	1340.46	16.18	0.00	**-16.18**	3.94
		0.04	53.94	**0.65**	-0.01	53.95	1334.90	7.07	0.00	**-7.07**	3.92
		0.05	67.25	**1.01**	-0.01	67.26	1326.85	12.92	0.00	**-12.92**	3.90
		0.06	80.49	**1.47**	-0.02	80.50	1321.74	9.58	0.00	**-9.58**	3.88
		0.07	93.66	**2.00**	-0.02	93.68	1314.20	10.73	0.00	**-10.73**	3.86
		0.075	99.97	**2.28**	-0.03	100.00	1311.74	7.55	0.00	**-7.55**	3.86

REFERENCES

[1] Silton, Sidra, "Comparison of Predicted Actuator Performance for Guidance of Supersonic Projectiles to Measure Range Data," 22nd Applied Aerodynamics Conference and Exhibit. Providence, RI, 2004.

[2] Anderson, John, *Modern Compressible Flow with Historical Perspective*, 2nd ed., Mcgraw-Hill Inc, New York, 1990, Chap. 4.

[3] F.S. Billig, "Shock Wave Shapes Around Cylindrical and Spherical Bodies," *Journal of Spacecraft and Rockets*, Vol. 4, 1967, pp 822-823.

[4] "An Exact, Explicit Method for Calculating the Shock Wave Angle for a Given Wedge Angle and Mach Number," *Journal of the Aero/Space Sciences*. Vol. 27, No. 1, 1960, pp. 71-73.

[5] CFD Research Corporation, "CFD-Fastran User's Manual Version 6.4," Huntsville, AL, 2001.

[6] CFD Research Corporation, "CFD-View User's Manual Version 6.4," Huntsville, AL, 2001.

[7] Arrow Tech Associate, "PRODAS User and Technical Manual," South Burlington, VT, 1997.